

1 **Seasonal cycles of biogeochemical fluxes in the Scotia Sea, Southern Ocean: A stable isotope**
2 **approach**

3

4 Anna Belcher¹, Sian F. Henley², Katharine Hendry^{1,3}, Marianne Wootton⁴, Lisa Friberg³, Ursula
5 Dallman², Tong Wang³, Christopher Coath³, Clara Manno¹

6 ¹ British Antarctic Survey, Cambridge, CB3 0ET, UK

7 ² School of GeoSciences, University of Edinburgh, Edinburgh EH9 3FE, UK

8 ³ University of Bristol, Bristol, BS8 1RJ, UK

9 ⁴ Marine Biological Association, Plymouth, PL1 2PB, UK

10

11 Correspondence to: Anna Belcher (annbel@bas.ac.uk) and Clara Manno (clanno@bas.ac.uk)

12

13 **Abstract**

14 The biological carbon pump is responsible for much of the decadal variability in the ocean carbon
15 dioxide (CO₂) sink, driving the transfer of carbon from the atmosphere to the deep ocean. A
16 mechanistic understanding of the ecological drivers of particulate organic carbon (POC) flux is key to
17 both the assessment of the magnitude of the ocean CO₂ sink, as well as for accurate predictions as to
18 how this will change with changing climate. This is particularly important in the Southern Ocean, a
19 key region for the uptake of CO₂ and the supply of nutrients to the global thermocline. In this study
20 we examine sediment trap derived particle fluxes and stable isotope signatures of carbon (C),
21 nitrogen (N) and biogenic silica (BSi) at a study site in the biologically productive waters of the
22 northern Scotia Sea in the Southern Ocean. Both deep (2000 m) and shallow (400 m) sediment traps
23 exhibited two main peaks in POC, particulate ~~nitrogen-N~~ and BSi flux, one in austral spring and one in
24 summer, reflecting periods of high surface productivity. Particulate fluxes and isotopic compositions
25 were similar in both deep and shallow sediment traps, highlighting that most remineralisation
26 occurred in the upper 400 m of the water column. Differences in the seasonal cycles of isotopic
27 compositions of C, N and Si provide insights into the degree of coupling of these key nutrients. We
28 measured increasing isotopic enrichment of POC and BSi in spring, consistent with fractionation
29 during biological uptake. Since we observed isotopically light particulate material in the traps in
30 summer, we suggest physically-mediated replenishment of lighter isotopes of key nutrients from
31 depth, enabling full expression of the isotopic fractionation associated with biological uptake. The
32 change in the nutrient and remineralisation regimes, indicated by the different isotopic
33 compositions of the spring and summer productive periods, suggests a change in the source region
34 of material reaching the traps and associated shifts in phytoplankton community structure. This,
35 combined with the occurrence of advective inputs at certain times of the year, highlights the need to
36 make synchronous measurements of physical processes to improve our ability to track changes in
37 the source regions of sinking particulate material. We also highlight the need to conduct particle-
38 specific (e.g. faecal pellet, phytoplankton detritus, zooplankton moults) isotopic analysis to improve

39 the use of this tool in assessing particle composition of the sinking material and to develop our
40 understanding of the drivers of biogeochemical fluxes.

41

42 1. Introduction

43 The transfer of carbon from the atmosphere to the deep ocean via the biological carbon pump (Volk
44 and Hoffert, 1985) is important for the sequestration of carbon, and combined with ocean
45 circulation is a main driver of decadal variability of the ocean carbon dioxide (CO₂) sink (DeVries,
46 2022). Mechanistic understanding of the processes controlling the magnitude and efficiency of the
47 biological carbon pump is therefore key to assessment and prediction of the ocean's role as a CO₂
48 sink and requires robust characterisation of the composition of the sinking particles transferring
49 particulate organic carbon (POC) to the deep ocean. The composition of particles affects the sinking
50 rate, lability and thus degree of remineralisation as they sink through the water column (e.g. Ploug
51 et al., 2008; Giering et al., 2020).

52 Sediment traps enable visual assessment of sinking particles, and have been deployed in numerous
53 locations throughout the world's oceans to both quantify biogeochemical fluxes and characterise the
54 nature of sinking material (~~for example data compilation of Atlantic Ocean sediment traps; e.g.~~
55 Torres Valdés et al., 2014). Sediment traps can be susceptible to collection biases depending on the
56 depth of deployment, trap design, hydrodynamic conditions and properties of sinking particles
57 (Buesseler et al., 2007). Moored sediment traps can underestimate the actual flux at depths
58 shallower than ~1500 m by collecting only a portion of the sinking material, though biases vary
59 greatly between sites (Buesseler et al., 2007). Numerous studies have recorded the dominance of
60 particular organisms or types of detrital material in trap material, highlighting the importance of
61 ecosystem community structure on the magnitude and efficiency of the biological carbon pump. For
62 example, faecal pellets, diatoms, diatom resting spores and acantharia have been observed as
63 significant contributors to particle fluxes (González et al., 2009; Belcher et al., 2018, 2017; Manno et
64 al., 2015; Gleiber et al., 2012; Rembauville et al., 2015; Roca-Marti et al., 2017). Such visual
65 assessment of trap material is typically very time consuming. Additionally, fragile material, such as
66 salp faecal pellets (Iversen et al., 2017; Pauli et al., 2021) may break up in the sample manipulation
67 processes, making them hard to account for visually. Biogeochemical methods such as the use of
68 stable isotopes may offer additional insight into the drivers of POC fluxes (e.g. Henley et al., 2012).

69 Marine phytoplankton take up aqueous CO₂ ($[CO_{2(aq)}]$) during photosynthesis, converting it to organic
70 carbon. During this process, the lighter isotope (¹²C) is preferentially assimilated, which enriches the
71 residual aqueous pool in the heavier isotope (¹³C). The stable isotopic composition of the POC
72 ($\delta^{13}C_{POC}$) of the marine phytoplankton is therefore lower than that of the carbon source. Over large
73 scales, the $\delta^{13}C$ of marine phytoplankton has been found to be inversely correlated with $[CO_{2(aq)}]$ in
74 surface waters (Rau et al., 1991). However, numerous other factors have been identified as
75 impacting the $\delta^{13}C_{POC}$ of surface waters and marine plankton. Phytoplankton growth rates, cell
76 geometry and non-diffusive uptake of carbon via carbon concentration mechanisms have all been
77 highlighted as impacting the $\delta^{13}C_{POC}$ of marine plankton and thus surface waters (Popp et al., 1999,
78 1998; Bidigare et al., 1999; Trull and Armand, 2001; Tuerena et al., 2019). This decoupling of the
79 relationship between $\delta^{13}C_{POC}$ and $[CO_{2(aq)}]$ presents challenges for palaeoceanographic studies, but

80 also the possibility of using the $\delta^{13}\text{C}_{\text{POC}}$ of marine samples to infer information about community
81 composition.

82 During photosynthetic uptake, the balance between supply and demand of carbon impacts $\delta^{13}\text{C}_{\text{POC}}$,
83 regulated by the transport of inorganic carbon into the internal cell and fixation to organic carbon
84 (Popp et al., 1999; Trull and Armand, 2001). A greater isotopic fractionation occurs in smaller
85 phytoplankton cells, enabled by the higher cell surface area to volume (SA:V) ratios and increased
86 amount of $[\text{CO}_{2(\text{aq})}]$ diffusing across the cell membrane relative to the total carbon within the cell
87 (Popp et al., 1998; Tuerena et al., 2019; Hansman and Sessions, 2016). Thus, a community
88 dominated by large, fast-growing diatoms is expected to contribute to enriched $\delta^{13}\text{C}_{\text{POC}}$ values
89 compared to a community dominated by picoplankton. A study by Henley et al. (2012) in the coastal
90 western Antarctic Peninsula, attributed a large ($\sim 10\text{‰}$) negative isotopic shift in $\delta^{13}\text{C}_{\text{POC}}$ to a near-
91 complete biomass dominance of the marine diatom *Proboscia inermis*, highlighting the possible
92 impact of shifts in species composition on stable isotopes. It may therefore be possible to use stable
93 isotopes to gain information about the community composition of phytoplankton driving, for
94 example, large spring pulses in POC flux. Additionally, siliceous phytoplankton, such as diatoms,
95 require dissolved silica (silicic acid, or DSi) to build their cell walls or frustules (amorphous $\text{SiO}_2 \cdot n\text{H}_2\text{O}$,
96 referred to here as biogenic silica, BSi). During uptake of DSi, diatoms fractionate the stable isotopes
97 of silicon (^{28}Si , ^{29}Si , ^{30}Si), preferentially taking up the lighter isotopes during cell wall (frustule)
98 formation (De La Rocha et al., 1997). This means that BSi fluxes and ratios of light ^{28}Si to heavy ^{30}Si
99 (expressed as $\delta^{30}\text{Si}$) in sinking particulate organic matter (POM) can be informative about DSi
100 utilisation by siliceous phytoplankton. The fractionation of Si isotopes during diatom DSi utilisation is
101 approximately -1.1‰ , although estimates of this value vary in laboratory and field studies between
102 -0.5 and -2.5‰ (Hendry and Brzezinski, 2014). Whilst some studies have shown that isotopic
103 fractionation is independent of temperature, DSi concentration and diatom species (e.g., De La
104 Rocha et al., 1997), one *in vitro* laboratory culture experiment revealed a potential species effect,
105 with polar species exhibiting more extreme fractionation (-2.09‰ for *Chaetoceros* sp. and 0.54‰
106 for *Fragilariopsis kerguelensis*; Sutton et al., 2013). The impact of water column dissolution on
107 frustule $\delta^{30}\text{Si}$ is poorly constrained, with experimental evidence for either a small fractionation of $-$
108 0.55‰ (Demarest et al., 2009) or a negligible impact (Wetzel et al., 2014; Egan et al., 2012; Grasse
109 et al., 2021).

110 Additionally, the stable isotopes of marine nitrogen reveal information about uptake of inorganic
111 nitrogen sources by phytoplankton (Wada and Hattori, 1978), as well as trophic and food web
112 processes (Michener and Lajtha, 2008). Nitrogen has two isotopes, ^{14}N and ^{15}N , and the ratio
113 between these heavy and light isotopes is expressed as $\delta^{15}\text{N}$. Different sources of nitrogen can alter
114 the stable isotopic composition of marine phytoplankton because ammonium characteristically has a
115 lower value of $\delta^{15}\text{N}$ than nitrate supplied from depth. As well as this, isotopic fractionation occurs
116 during transfer through the food web, with a trophic enrichment of typically $2-4\text{‰}$ between
117 successive trophic levels (Montoya, 2007; Minagawa and Wada, 1984). Excretion and egestion
118 processes can also impact $\delta^{15}\text{N}$; isotopic discrimination during excretion of ammonium by
119 zooplankton and fish results in ammonium that is ^{15}N -depleted relative to the substrate catabolised
120 (Montoya, 2007). Thus, there are several interacting processes impacting the degree of fractionation
121 and subsequent isotopic ratios in particulate nitrogen (PN) and knowledge of $\delta^{15}\text{N}$ ratios may
122 provide insight into biogeochemical processes and the composition of the sinking flux.

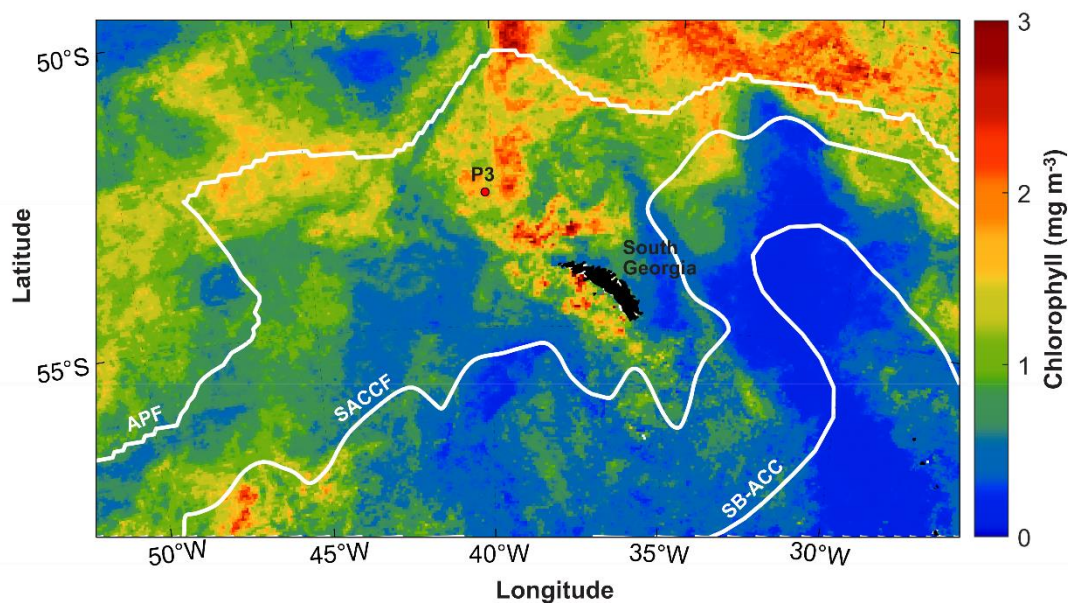
123 In this study we examine the seasonal cycle of the magnitude and composition of vertical
124 biogeochemical fluxes of particulate material collected by two sediment traps deployed for almost
125 one year on a deep ocean mooring located in the northern Scotia Sea in the Atlantic sector of the
126 Southern Ocean. The Scotia Sea, particularly the region downstream of South Georgia, is a hot spot
127 for biological productivity, supported by higher iron availability (Korb et al., 2008; Matano et al.,
128 2020). Diatoms dominate the phytoplankton assemblage, particularly in the summer months, with
129 smaller contributions of dinoflagellates (Korb et al., 2012). The large, consistent phytoplankton
130 blooms occurring in this region support high fluxes of POC to the deep ocean, with two peaks in POC
131 flux occurring during the seasonal cycle; **the** first peak in austral spring, and **the** second in late
132 summer or early autumn (Manno et al., 2015). Faecal pellets (up to 91 % in late spring and early
133 summer; Manno et al., 2015), krill exuviae (up to 47 % in summer; Manno et al., 2020) and diatoms,
134 particularly resting spores (annual contribution of 42 %; Rembauville et al., 2016) have been shown
135 to make large contributions to the POC fluxes in our study region. Here we use $\delta^{13}\text{C}_{\text{POC}}$, $\delta^{15}\text{N}_{\text{PN}}$ and
136 $\delta^{30}\text{Si}_{\text{BSi}}$ alongside calculated fluxes of POC, PN and BSi as tools to reveal information about sinking
137 particulate organic matter and the processes influencing its production and subsequent flux to
138 depth. More in-depth understanding of the composition, and thus the drivers of POC flux in this
139 important region are key to improving estimates of the current and future strength of the biological
140 carbon pump and the ocean's role as a CO_2 sink.

141

142 2. Methods

143 2.1. Study Area

144 This study was conducted in the open ocean environment of the northern Scotia Sea in the Southern
145 Ocean at a long-term observatory station, P3 (Figure 1), where an oceanographic mooring is located.
146 The mooring is part of the Scotia Sea Open Ocean Observatory (SCOOBIES:
147 <https://www.bas.ac.uk/project/scoobies/>), a programme designed to investigate the biological and
148 biogeochemical influence of the large and persistent phytoplankton bloom to the northwest of
149 South Georgia.



150

151 **Figure 1: Location of P3 mooring site to the northwest of South Georgia. White lines indicate**
152 **frontal positions of the Antarctic Polar Front (APF) (Moore et al., 1999), Southern Antarctic**
153 **Circumpolar Current Front (SACCF) (Thorpe et al., 2002) and the Southern Boundary of the**
154 **Antarctic Circumpolar Current (SB-ACC) (Orsi et al., 1995). Mean chlorophyll concentration (mg m^{-3})**
155 **is shown for December 2018 from 8-day satellite chlorophyll data from the Ocean Colour CCI**
156 **(version 5.0) (Sathyendranath et al., 2021, 2019).**

157

158 2.2. Sediment trap deployment

159 Two sediment traps were deployed on the mooring array to collect sinking particles for analysis of
160 carbon, nitrogen and biogenic silica fluxes and analysis of $\delta^{13}\text{C}_{\text{POC}}$, $\delta^{15}\text{N}_{\text{PN}}$ and $\delta^{30}\text{Si}_{\text{BSi}}$. The mooring
161 was deployed from 25th January 2018, during research cruise JR17002 aboard the *RRS James Clark*
162 *Ross*, to 1st January 2019, recovered during research cruise DY098 aboard the *RRS Discovery*. The
163 mooring was located at 52.8036 °S, 40.1593 °W, to the northwest of South Georgia island in the
164 Scotia Sea at a water depth of 3748 m. Sediment traps (McLane PARFLUX, 0.5 m² surface collecting
165 area; McLane [Research Laboratories Inc](#), Falmouth, MA, USA) were deployed at 400 and 2000 m
166 (referred to hereafter as shallow and deep respectively) and were each equipped with 21
167 sample bottles. A baffle at the top of the trap prevents large organisms from entering and each
168 sample bottle contained a formosaline solution (filtered seawater containing 2 % v/v formalin, mixed
169 with sodium tetraborate (BORAX; 0.025 % w/v), and 0.5% w/v sodium chloride) to prevent mixing
170 with the overlying water column and stop biological degradation. Previous studies have reported the
171 effects of formalin on $\delta^{13}\text{C}_{\text{POC}}$ and $\delta^{15}\text{N}_{\text{PN}}$ to be small (± 1 ‰ and ± 1.5 ‰ respectively; Mincks et al.,
172 2008 and references therein). This equates to 13 % and 16 % of the maximum range measured in our
173 study, which is small compared to the isotopic shifts we observed. Yet we stress that all $\delta^{13}\text{C}_{\text{POC}}$ and
174 $\delta^{15}\text{N}_{\text{PN}}$ values given here are associated with this uncertainty. The sediment trap sample carousel
175 was programmed to rotate every 7-31 days depending on the season; shorter periods to coincide
176 with austral summer and longer periods during austral winter (Table S1). TM Seaguard current
177 meters were deployed ~50 m above the shallow sediment trap and 50 m below the deep sediment
178 trap, set at a measurement interval of 2 hours.

179 2.3. Trap sample processing

180 Each sample bottle from the sediment trap was processed on return to the laboratory. The
181 supernatant was carefully removed using a syringe and swimmers (zooplankton that are believed to
182 have entered the trap actively whilst alive) were removed. Swimmers were removed by hand under
183 a dissecting microscope and were not included in flux calculations. The material from each sediment
184 trap sample bottle was split into a number of smaller aliquots for subsequent analysis using a
185 McLane rotary splitter.

186

187 2.3.1. Organic carbon and nitrogen

188 For each sediment trap bottle from both deep and shallow traps, two or three splits were taken and
189 each analysed for POC and PN mass and $\delta^{13}\text{C}_{\text{POC}}$ and $\delta^{15}\text{N}_{\text{PN}}$. Once split, the material was filtered onto
190 pre-combusted (450 °C, 16h) 25 mm glass fibre filters (GF/F; nominal pore size 0.7 μm) and rinsed
191 with milli-Q water. Samples were air dried, fumed for 24 h with 37 % HCl in a desiccator, before

192 finally oven-drying at 50 °C for 24 h. Filters and filter blanks were placed in sterile tin capsules and
193 POC and PN were measured on a CE Instruments NA2500 ~~E~~elemental analyser, calibrated using an
194 acetanilide calibration standard with a known %C and %N of 71.09 % and 10.36 % respectively.
195 Standards were interspersed regularly between samples to measure and correct for drift. Analytical
196 precision was better than 1.0 % for POC and 1.1 % for PN. The POC flux (F , $mg\ C\ m^{-2}\ d^{-1}$) for each
197 sample was calculated using the following equation:

$$198\quad F = m/(A \times d) \quad (1)$$

199 Here m is the mass of POC in the sample bottle (mg), d is the number of days that the sample bottle
200 was open (7–31 days) and A is the surface area of the sediment trap opening ($0.5\ m^2$). The same
201 calculation was carried out for PN.

202 $\delta^{13}C_{POC}$ and $\delta^{15}N_{PN}$ were analysed on a Thermo Finnigan Delta-~~V~~Plus Advantage isotope ratio mass
203 spectrometer that was in line with the elemental analyser. All $\delta^{13}C_{POC}$ and $\delta^{15}N_{PN}$ data are presented
204 in the delta per mille (‰) notation relative to the appropriate international standard, according to
205 equation 2.

$$206\quad \delta X(\text{‰}) = 10^3 (R_{sample}/R_{standard} - 1) \quad (2)$$

207 R denotes the $^{13}C/^{12}C$ ratio for carbon or the $^{15}N/^{14}N$ ratio for nitrogen. R_{sample} refers to the relevant
208 ratio in the sample. $R_{standard}$ refers to the ratios in the international standards Vienna Pee Dee
209 belemnite (V-PDB) for $\delta^{13}C$ and atmospheric nitrogen (AIR) for $\delta^{15}N$, both of which are calibrated
210 against the PACS-2 marine sediment reference material. Multiple repeats of analytical standards
211 gives a reproducibility of 0.2 ‰ for C and N, which is significantly smaller than the uncertainty
212 associated with organic carbon molecules in the formalin preservative ($\pm 1\ \text{‰}$ and $\pm 1.5\ \text{‰}$ for C and
213 N respectively; Mincks et al., 2008 and references therein).

214

215 2.3.2. Biogenic silica

216 Two splits were taken from each sample bottle from both deep and shallow sediment traps for
217 analysis of biogenic silica and silicon isotopes. Split material was filtered onto 25 mm, $0.4\ \mu m$,
218 polycarbonate filters and rinsed with Milli-Q water before drying at 50 °C for 24h. Material on the
219 filters was solubilised via an alkaline extraction method (Hatton et al., 2019) carried out at the Bristol
220 Isotope Group (BIG) laboratory. Sample material was digested in Teflon tubes with 0.2M NaOH at
221 100 °C for 40 minutes. This was followed by neutralisation with 6M HCl. Biogenic silica (SiO_2 , termed
222 BSi) concentrations were measured chlorometrically by molybdate blue spectrophotometry
223 (Heteropoly Blue Method) (Strickland and Parsons, 1972) using a Hach DR3900 spectrophotometer
224 set at a wavelength of 815 nm. Supernatants were stored for 7-11 months before column chemistry
225 for isotope analysis. Fluxes of biogenic silica were calculated as for POC using equation 1.

226 For Si isotope analysis, supernatants and reference materials were purified by passing through
227 cation exchange columns (Bio-Rad AG50W-X12, 200-400 mesh resin) pre-cleaned with HCl following
228 Georg et al. (2006). Samples were acidified to a pH of 1-2 to ensure that all the silicon remained in
229 solution. Samples were loaded onto columns and eluted with Milli-Q water to produce a 2.5 ppm
230 solution, and concentrations were checked to confirm quantitative yields. Si isotopic composition
231 was analysed within 24 hours of column chemistry. Stable Si isotopic compositions are presented in

232 standard delta notation ($\delta^{30}\text{Si}$), as for $\delta^{13}\text{C}_{\text{POC}}$ and $\delta^{15}\text{N}_{\text{PN}}$ according to Equation 2, where R is $^{30}\text{Si}/^{28}\text{Si}$.
233 These compositions are checked against $\delta^{29}\text{Si}$ (where R is $^{29}\text{Si}/^{28}\text{Si}$) for mass dependence. The
234 samples were measured at the BIG laboratory on a Finnigan Neptune Plus High-Resolution MC-ICP-
235 MS (Thermo Fisher Scientific). The Si solutions were spiked with magnesium spike (Inorganic
236 Ventures MSMG-10 ppm), hydrochloric acid (1M HCl in-house distilled) and sulphuric acid (0.1M
237 H_2SO_4 , ROMIL-UpA™ Ultra Purity Sulphuric Acid), and transferred from the autosampler via a PFA
238 Savillex C-Flow nebulizer ($35 \mu\text{l min}^{-1}$) connected to an Apex IR Desolvating Nebulizer (Ward et al.,
239 2022), and measured on the low-mass side to resolve any isobaric interferences (e.g., $^{14}\text{N}^{16}\text{O}^+$). All
240 standards and samples were blank-corrected offline. The intensity of ^{28}Si in the 0.1M HCl blank was
241 $<1\%$ of the sample intensity in all sample runs. Furthermore, we also measured Mg isotopes (^{24}Mg ,
242 ^{25}Mg and ^{26}Mg) as an internal isotopic reference to correct for any mass-dependent fractionation
243 (Cardinal et al., 2003)(White et al., 2000). Measurements that resulted in large corrections ($>0.3\%$
244 on $\delta^{30}\text{Si}$) underwent repeat analysis. Instrumental mass bias was further accounted for using a
245 standard-sample bracketing method using a 2 ppm reference standard (NBS or RM8546) solution.
246 Two splits were analysed for each sediment trap bottle, as well as standards and sample blanks.
247 Solutions obtained from each split were measured in replicate ($n = 2-3$) alongside continuous
248 measurement of reference materials Diatomite and LMG-08 to ensure reproducibility and to
249 monitor data quality. Measurements of Diatomite and LMG-08 yielded $\delta^{30}\text{Si}$ of $+1.23\%$ (SD ± 0.03 ,
250 $n=18$) and -3.40% (SD ± 0.05 , $n=5$) respectively, which agreed with published values (Reynolds et
251 al., 2007; Hendry and Robinson, 2012; Grasse et al., 2017). Typical reproducibility between the
252 sediment trap sample splits (coming from the same sediment trap bottle) was 0.034% ($1 \times \text{SD}$). A
253 lithogenic correction (e.g., Closset et al., 2015) was not carried out on these samples given the high
254 percentage of biogenic silica present in the samples (mean percentage BSi as SiO_2 of 17 %). BSi
255 extraction methods show lower variability for marine sediments with BSi $> 15-20\%$ and do not show
256 evidence for significant leaching of lithogenic material through time (Conley, 1998). However, even
257 an extreme scenario of variable lithogenic contamination of 1-5 % of isotopically light marine clays
258 (with $\delta^{30}\text{Si}$ of -2.3% ; Opfergelt and Delmelle, 2012) would only result in a potential systematic
259 offset of 0.12% , which, although this is larger than the uncertainty on an individual datapoint, is an
260 order of magnitude smaller than the observed seasonal signal.

261 2.4. *Chlorophyll and phytoplankton community composition*

262 Surface chlorophyll concentrations were obtained from satellite-derived 8-day Ocean Colour CCI
263 (version 5.0) (Sathyendranath et al., 2021, 2019). We present the monthly mean of these 8-day data
264 for December at our study site (Figure 1), as well as the 8-day chlorophyll concentration data from
265 September 2017 to December 2018 (Figure 2) averaged over a $1 \times 1^\circ$ bounding box around our study
266 site (41°W , 40°W , 53°S , 52°S).

267 Light microscopy was used to assess phytoplankton and microzooplankton community composition
268 of a small selection of samples from the two main productive periods. A biological method of sample
269 preparation and analysis was chosen, comparable with Rembauville et al. (2015), to determine the
270 quantity of empty and full cells. Following subsampling using the rotary splitter, samples for
271 morphological taxonomic analysis were diluted to a standardised 25 ml. Samples were gently
272 inverted using the Paul Schatz principle (figures of eight) for one minute to homogenise them, and 2
273 ml was withdrawn using a modified pipette with widened opening. Several common diatoms in
274 Antarctic waters are long and slim; in particular, *Thalassiothrix antarctica* has been recorded with an

275 apical axis up to 5mm. To ensure such specimens remain intact and are not excluded from the
276 pipetting process, a wide bore opening ~~is necessary~~ was used. The 2 ml subsamples were used to fill
277 a 1 ml Sedgwick Rafter counting chamber. Chambers were viewed using a compound light
278 microscope (Nikon Eclipse 80i) with differential interference contrast at x200 magnification. For the
279 larger, easily identifiable cells, the whole chamber was observed; for smaller cells a proportion of the
280 chamber was examined depending upon cell abundance (at least 500 cells were counted). Only
281 complete cells were enumerated to avoid over counting of fragmented specimens. Cells were
282 determined as “full” or alive at time of collection if they possessed chloroplasts/plastids, pigment, a
283 nucleus or, in the case of *Pronoctiluca*, a distinct accumulation body; cells lacking these internal
284 features were deemed as “empty”, or dead at time of collection. Specimens were identified
285 according to Hasle and Syvertsen (1997), Medlin and Priddle (1990), Priddle and Fryxell (1985) and
286 Scott and Marchan (2005).

287 Cell bio-volume and surface area estimates were calculated using geometrics and the appropriate
288 shape-related equations for phytoplankton genera proposed by Hillebrand et al. (1999). Metrics
289 used in the calculations were based on the average size of ten randomly selected specimens
290 belonging to a species ~~or other~~ taxonomic group within the samples.

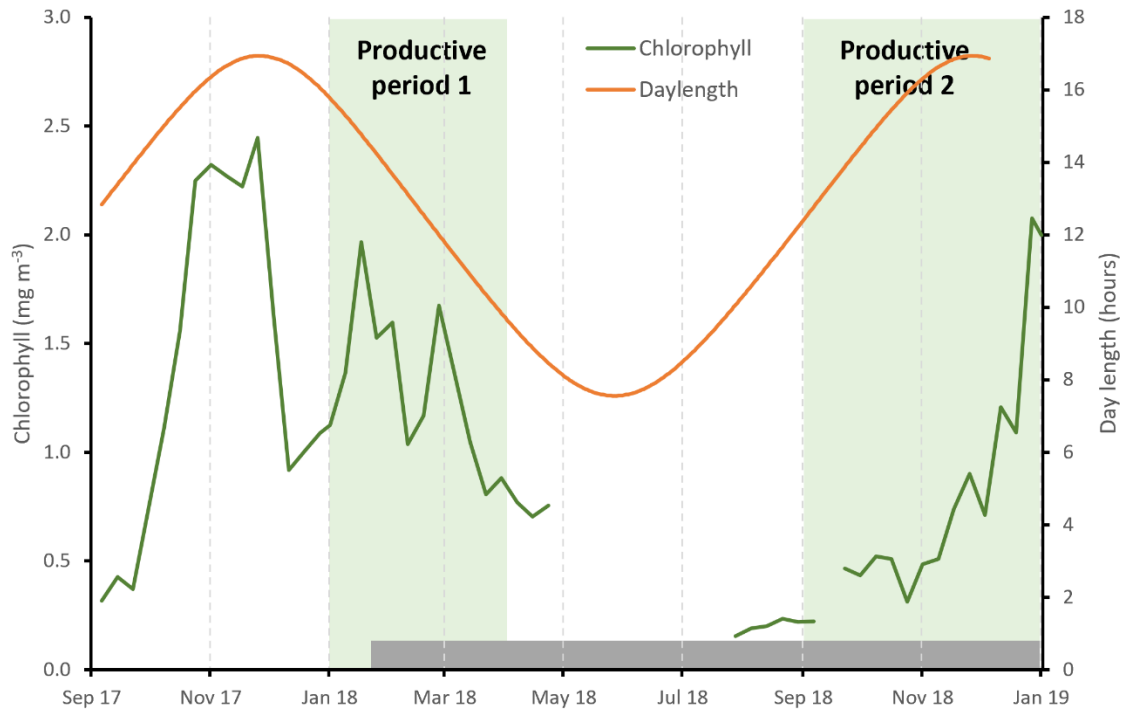
291

292 3. Results

293 3.1. Environmental conditions

294 Mean current velocities were 0.11 (± 0.06) and 0.06 (± 0.03) m s⁻¹ for shallow and deep current
295 meters respectively (Supplementary Figure S1). Maximum current speeds recorded reached 0.43
296 and 0.18 m s⁻¹ for shallow and deep meters respectively. The periods with currents substantially
297 elevated above the mean were June for both traps, and additionally in late August/September for
298 the shallow trap, both for periods of ~5-10 days. Both are periods of low fluxes during austral winter
299 and are not the main subject of the study here, though it is likely that particle collection was biased
300 at these times (Buesseler et al., 2007).

301 Satellite-derived estimates of surface chlorophyll show high concentrations during austral summer
302 (January to March) peaking at 2.3 mg m⁻³, as well as during spring (November-December), peaking at
303 2.1 mg m⁻³ (Figure 2, Figure S2). Data coverage is limited in the winter due to cloud cover, but
304 concentrations appear to be <0.4 mg m⁻³. We define here two productive periods (when chlorophyll
305 concentrations were >0.4 mg m⁻³), which we refer to throughout the manuscript, productive period
306 1: January to the start of April 2018, and productive period 2: September to the end of December
307 2018. We note that our sediment trap data begins on the 25th January so we do not capture the start
308 of period 1.



309

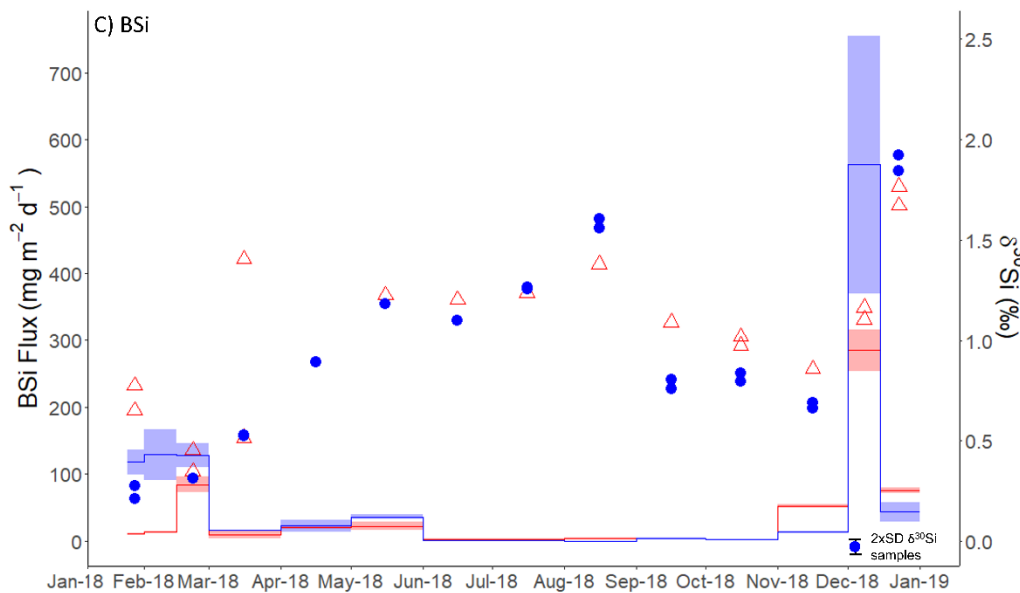
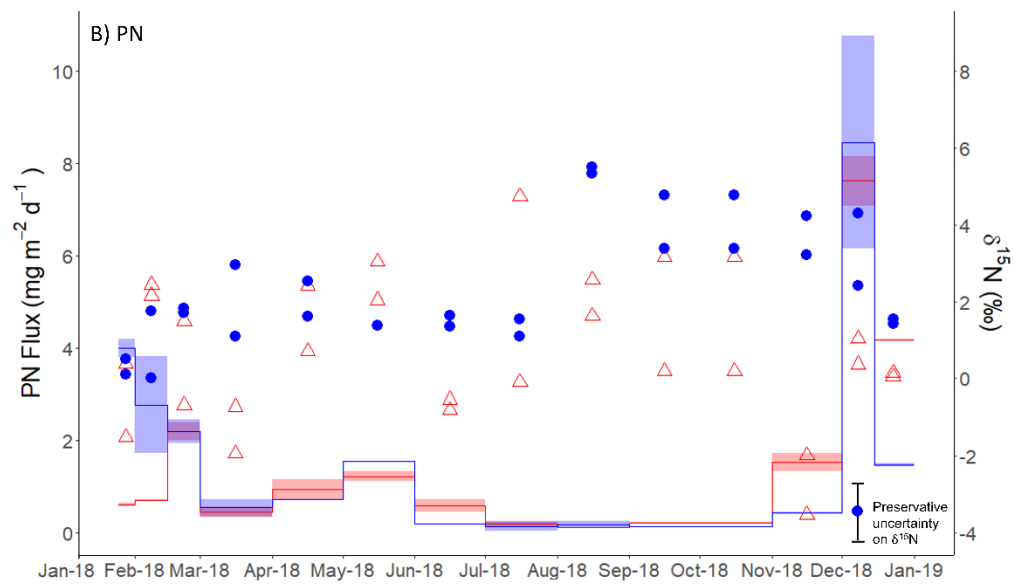
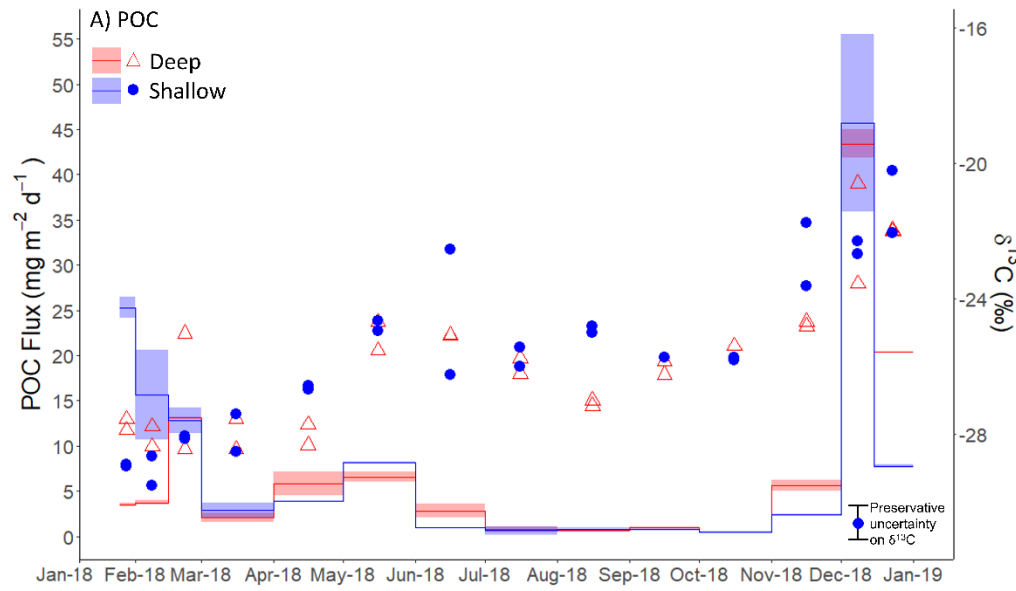
310 **Figure 2: Seasonal cycle of satellite derived surface chlorophyll concentration (green line, 8-day**
 311 **data from the Ocean Colour CCI (version 5.0)) (Sathyendranath et al., 2021, 2019)). Daylength at 53**
 312 **°S is shown by the orange line. The two productive periods are highlighted by the shaded green**
 313 **regions, and the grey shaded bar shows the duration of the sediment trap ~~was opensampling~~**
 314 **period.**

315

316 3.2. POC, PN, BSi fluxes

317 There is a clear seasonal cycle in POC, PN and BSi fluxes, all tracking each other well (Figure 3). Since
 318 two to three splits were analysed from each sediment trap bottle, we refer here to the mean flux for
 319 each sediment trap bottle based on the available splits for that bottle. POC fluxes were low during
 320 austral autumn and winter, with fluxes $<10 \text{ mg C m}^{-2} \text{ d}^{-1}$ and $<7 \text{ mg C m}^{-2} \text{ d}^{-1}$ for shallow and deep
 321 traps respectively during the period March to October 2018 (Figure 3A). Higher fluxes were
 322 measured in summer 2018 (productive period 1), reaching $25.3 \text{ mg C m}^{-2} \text{ d}^{-1}$ in late January 2018 in
 323 the shallow trap and $13.1 \text{ mg C m}^{-2} \text{ d}^{-1}$ in late February in the deep trap. The maximum POC fluxes
 324 measured occurred in early December 2018 (productive period 2), reaching $45.7 \text{ mg C m}^{-2} \text{ d}^{-1}$ and
 325 $43.4 \text{ mg C m}^{-2} \text{ d}^{-1}$, in shallow and deep traps respectively. PN fluxes follow the same trends as POC
 326 fluxes, peaking at 4.2 and $2.4 \text{ mg N m}^{-2} \text{ d}^{-1}$ during period 1, and 10.8 and $8.2 \text{ mg N m}^{-2} \text{ d}^{-1}$ during
 327 period 2, in shallow and deep traps respectively (Figure 3B). The mean POC:PN ratio (mol:mol)
 328 throughout the study period was $6.40 (\pm 0.73)$ and $6.02 (\pm 0.90)$ in shallow and deep traps
 329 respectively, with higher ratios in the productive periods compared to the winter months. Mean
 330 POC:PN ratios were $6.8375 (\pm 0.486)$ and $6.63 (\pm 0.71)$ during period 1 and period 2 in the shallow
 331 trap, and $6.4064 (\pm 0.635)$ and $5.51 (\pm 0.87)$ in the deep trap. Over the winter months POC:PN was
 332 $5.683 (\pm 0.54)$ and $5.926.26 (\pm 0.87)$ in shallow and deep traps respectively.

333 BSi fluxes (Figure 3C) track those of POC well. Lowest fluxes ($<20 \text{ mg SiO}_2 \text{ m}^{-2} \text{ d}^{-1}$, ~~except a small peak~~
334 ~~of up to $39.7 \text{ mg SiO}_2 \text{ m}^{-2} \text{ d}^{-1}$ in May 2018~~) occurred in the autumn/winter (March-October), with the
335 exception of a small peak of up to $39.7 \text{ mg SiO}_2 \text{ m}^{-2} \text{ d}^{-1}$ in May 2018. During summer 2018
336 (productive period 1), BSi fluxes were high, reaching $129.1 \text{ mg SiO}_2 \text{ m}^{-2} \text{ d}^{-1}$ in early February in the
337 shallow trap and $84.3 \text{ mg SiO}_2 \text{ m}^{-2} \text{ d}^{-1}$ in late February in the deep trap. By far the highest fluxes were
338 observed in spring 2018 (productive period 2), peaking in early December at $562.4 \text{ mg SiO}_2 \text{ m}^{-2} \text{ d}^{-1}$,
339 and $285.4 \text{ mg SiO}_2 \text{ m}^{-2} \text{ d}^{-1}$ in shallow and deep traps respectively. The mean BSi:POC ratio (mol:mol)
340 throughout the study period was $29.82 (\pm 17.80)$ and $25.86 (\pm 11.72)$ in shallow and deep traps
341 respectively. Higher BSi:POC ratios were observed in the shallow trap in period 1 (38.45 ± 10.96), and
342 both shallow and deep traps in period 2 (36.94 ± 16.32 and 35.70 ± 12.10 respectively). BSi:POC ratios
343 were lower in the deep trap during period 1 (23.64 ± 6.82). The ~~match-correspondence~~ in timing of
344 elevated fluxes of POC, PN and BSi fluxes in the shallow and deep traps in spring (period 2) highlights
345 that sinking rates must be sufficient ($>114 \text{ m d}^{-1}$) for particles to travel the 1600 m between the two
346 traps in the 14 day period that those sediment trap cups were open. In period 1, there was a time lag
347 of 14 to 35 days between the timing of the maximum POC, PN, and BSi fluxes in the deep and
348 shallow sediment traps. This suggests sinking rates of 46-114 m d^{-1} . However, we stress that this
349 assumes vertical sinking, which as we discuss in Section 4 is not always the case.



351 **Figure 3: A) Particulate organic carbon (POC), B) particulate nitrogen (PN) and C) biogenic silica**
 352 **(SiO₂, BSi) fluxes (mg m⁻² d⁻¹) at deep (red shading) and shallow (blue shading) sediment traps.**
 353 **Shading indicates the maximum and minimum flux from two splits, with the solid line indicating**
 354 **the mean value. Coloured points show isotope ratios for A) δ¹³C_{POC}, B) δ¹⁵N_{PN} and C) δ³⁰Si_{BSi} with red**
 355 **open triangles and blue filled circles indicating deep and shallow sediment traps, respectively. [The](#)**
 356 **[legend shown in the top left hand corner of panel A applies to all panels.](#) The maximum error on**
 357 **sediment trap δ¹³C_{POC} (±1 ‰) and δ¹⁵N_{PN} (±1.5 ‰) values are shown by scaled error bars in the**
 358 **bottom right corner, and are associated with formaldehyde preservation (Mincks et al., 2008) since**
 359 **this vastly exceeds analytical error. For δ³⁰Si_{BSi}, the scaled error bar represents 2 x SD (0.07 ‰-0.7)**
 360 **for the analytical sample replicates. For each sample, isotope ratios are given at the midpoint of**
 361 **the period that the sample cup was open.**

362 3.3. δ¹³C_{POC}, δ¹⁵N_{PN} and δ³⁰Si_{BSi} Isotopes

363 δ¹³C_{POC} values of deep and shallow sediment trap samples track each other well and show the same
 364 order of enrichment and depletion (Figure 3A). ~~Again, when~~ [When presenting-describing](#) the results
 365 for an individual sediment trap bottle, we give the mean of replicate splits from that sediment trap
 366 bottle unless otherwise stated. Initially, from January to March 2018, we see isotopically light δ¹³C_{POC}
 367 values between -27.40 and -28.56 ‰, before increasing to -24.38 ‰ and -25.07 ‰ in June in shallow
 368 and deep traps respectively. Over winter, δ¹³C_{POC} became more depleted (shallow: -25.76 ‰ in
 369 October, deep -27.07 ‰ in August) with a slight divergence (2.17 ‰) in the tracking of deep and
 370 shallow δ¹³C_{POC} in August 2018. Coinciding with increasing chlorophyll concentrations, δ¹³C_{POC}
 371 became more enriched during the period September to December 2018 (-25.72 to -21.13 ‰ and -
 372 26.04 to -21.98 ‰ for shallow and deep traps respectively).

373 Comparison of flux-weighted δ¹³C_{POC} values confirms the carbon isotopic similarity of deep and
 374 shallow traps, particularly during period 2 (Table 1). These results also highlight the shift in both
 375 δ¹³C_{POC} and δ³⁰Si_{BSi} between period 1 and period 2.

376 **Table 1: Sediment trap seasonal (Jan 2018 – Dec 2018), period 1 (Jan 2018 – start of April 2018),**
 377 **~~and~~ period 2 (Sept 2018- – end of Dec 2018), and winter (April – end of August) flux-weighted**
 378 **mean δ¹³C_{POC} (‰), δ¹⁵N_{PN} (‰) and δ³⁰Si_{BSi} (‰) for shallow (400 m) and deep (2000 m) traps. Given**
 379 **that the analytical conditions were the same for all samples measured, we use the pooled variance**
 380 **over the applicable time period as a measure of uncertainty on these mean isotopic ratios. Degrees**
 381 **of freedom (dof) are based on cups with replicate isotopic measurements and are given in**
 382 **parentheses.**

Time period	δ ¹³ C _{POC} (‰)		δ ¹⁵ N _{PN} (‰)		δ ³⁰ Si _{BSi} (‰)	
	Shallow	Deep	Shallow	Deep	Shallow	Deep
Seasonal	-25.15 ±0.49 (dof=14)	-24.40 ±0.45 (dof=14)	2.07 ±0.34 (dof=14)	0.39 ±0.43 (dof=14)	0.50 ±0.09 (dof=8)	0.86 ±0.10 (dof=6)
Period 1	-28.5930 ±0.341 (dof=45)	-27.2452 ±0.4133 (dof=45)	1.160.98 ±0.4036 (dof=45)	0.7153 ±0.6658 (dof=45)	0.215 ±0.0109 (dof=2)	0.5947 ±0.163 (dof=2)
Period 2	-22.47 ±1.03 (dof=5)	-22.79 ±0.74 (dof=5)	2.97 ±0.66 (dof=5)	-0.09 ±0.65 (dof=5)	1.54 ±0.30 (dof=4)	1.08 ±0.14 (dof=4)

Winter	<u>-25.31 ±0.63</u> (dof=5)	<u>-26.25 ±0.39</u> (dof=5)	<u>1.81 ±0.49</u> (dof=5)	<u>1.74 ±0.64</u> (dof=5)	<u>0.58 ±0.20</u> (dof=2)	<u>0.48 ±0.17 (*)</u>
--------	--------------------------------	--------------------------------	------------------------------	------------------------------	------------------------------	-----------------------

383 * There were no replicates from the deep sediment trap sample bottles for Si isotopes during this
384 period.

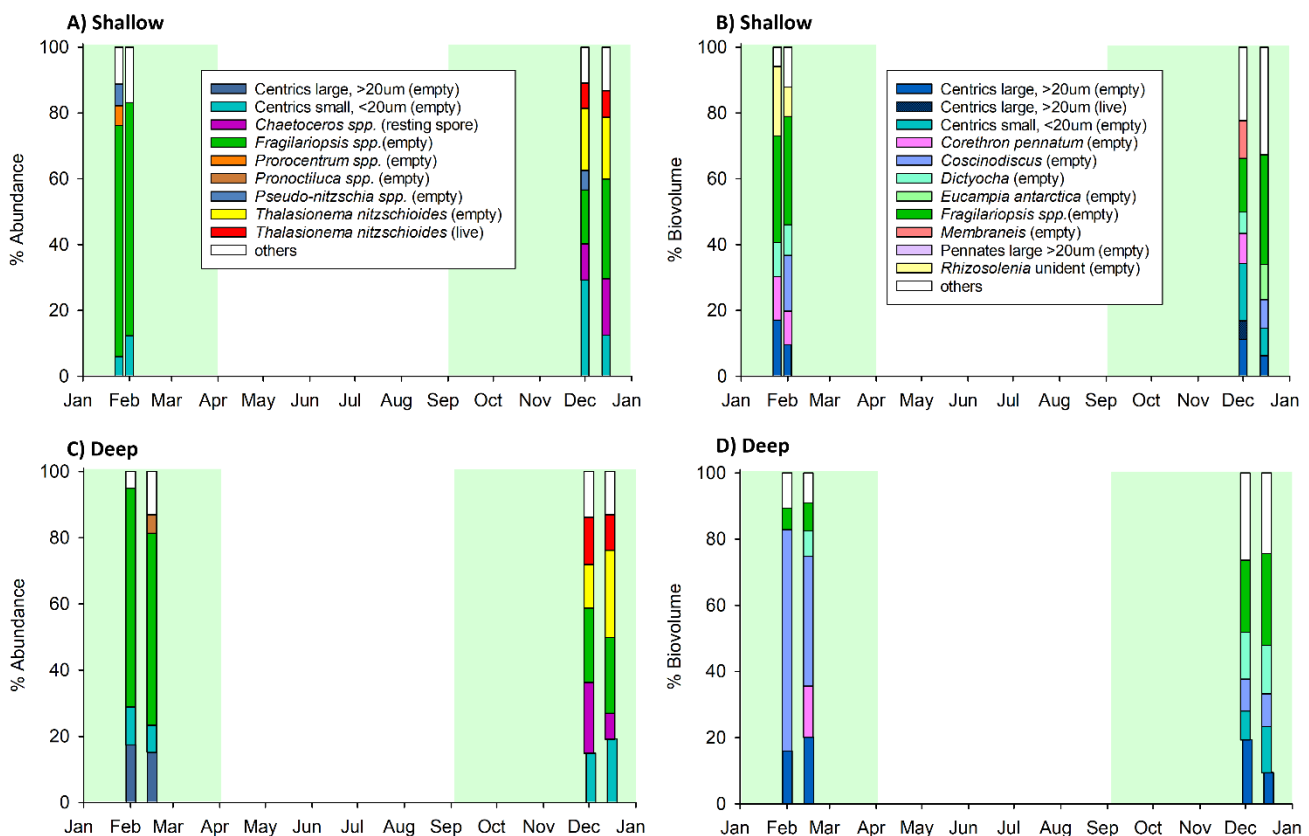
385 $\delta^{15}\text{N}_{\text{PN}}$ values are less consistent between deep and shallow sediment trap samples and there is
386 more heterogeneity between sample splits. For the shallow trap we see values ranging between
387 +0.13 and +2.96 ‰ (mean +1.42 ‰, SD 0.79 ‰) from January to June 2018, and, for the deep trap,
388 values ranged between -1.95 and +3.04 ‰ (mean +0.60 ‰, SD 1.60 ‰) during this period. Values
389 increase between June and August, reaching +5.42 and +2.10 ‰ in shallow and deep traps
390 respectively. From August to December (shallow), and August to November (deep), we see a trend
391 of decreasing $\delta^{15}\text{N}_{\text{PN}}$ to +1.49 and -2.77 ‰ in shallow and deep traps respectively, with the decrease
392 being of similar magnitude (3.93 and 4.87 ‰ respectively) for both traps. Shallow $\delta^{15}\text{N}_{\text{PN}}$ ~~are~~ is
393 consistently higher than deep $\delta^{15}\text{N}_{\text{PN}}$ by 4.52 ‰ on average during this period (August to November).
394 In the deep trap we see a final increase in $\delta^{15}\text{N}_{\text{PN}}$ coinciding with the increase in PN flux from
395 November to December 2018, reaching a mean of +0.71 ‰. The same increase in $\delta^{15}\text{N}_{\text{PN}}$ is not
396 apparent in the shallow trap.

397 Si isotope compositions in deep and shallow samples were quite similar, exhibiting the same
398 seasonal patterns. Both deep and shallow traps showed an increase in $\delta^{30}\text{Si}_{\text{BSi}}$ from January to July
399 2018 (+0.71 to +1.24 ‰ in the deep trap, and +0.24 to +1.26 ‰ in the shallow trap) with the
400 steepest increase occurring from March to May (Figure 3C). Sample splits generally showed good
401 agreement with one exception during March 2018 when sample splits from the deep sediment trap
402 were +0.52 and +1.41 ‰, highlighting the heterogeneous nature of the sediment trap material.
403 Isotopic values in the deep trap were then quite steady over winter compared to the rest of the
404 record, with an increase of 0.38 ‰ in the shallow trap between May and August. At the ~~until the~~ end
405 of August, ~~when~~ $\delta^{30}\text{Si}_{\text{BSi}}$ began to decrease steeply, reaching +0.68 and +0.86 ‰ in shallow and deep
406 traps respectively in November 2018. Following this, $\delta^{30}\text{Si}_{\text{BSi}}$ increased rapidly to +1.72 (deep) and
407 +1.89 ‰ (shallow) coinciding with the large increase in BSi fluxes at this time.

408 3.4. Phytoplankton community structure

409 Eight samples (four deep and four shallow, Itable 2) were analysed by light microscopy for
410 phytoplankton composition to cover the high productivity periods 1 and 2. Diatoms, silicoflagellates
411 and dinoflagellates were observed, with a dominance of diatoms (>85% by both abundance and
412 biovolume). Micro-zooplankton were also recorded, in particular radiolarians and tintinnids, though
413 these were not dominant by biovolume or abundance. Only intact cells were identified and counted.
414 In terms of abundance, during period 1, the diatoms *Fragilariopsis spp.* dominated both deep (58-66
415 %) and shallow (~70 %) trap samples (Figure 4A, C), whereas during period 2 the phytoplankton
416 community structure was more mixed with contributions from the diatoms *Thalassionema*
417 *nitzschioides*, *Chaetoceros*, small (<20 μm) centrics, as well as *Fragilariopsis spp.* Large centric
418 diatoms (>20 μm) represented 15-20 % of the community by abundance in the deep trap during
419 productive period 1, but <2.5 % in productive period 2. Interestingly we do not see these large
420 centrics in the shallow trap during productive period 1, implying that sinking velocities were < 76 m
421 d^{-1} for these large phytoplankton cells based on the duration that the first sediment trap bottle was
422 open and the depth between the two traps.

423 In terms of biovolume, *Fragilariopsis spp.* were still a dominant component of the shallow trap
 424 sample in period 1 (~33 %) but were <9 % of the community in the deep trap during period 1, with
 425 the large cells of the diatom *Coscinodiscus* dominating with 39-67 % (Figure 4B, D). Diatoms,
 426 *Corethron pennatum* (shallow: 10-13 %; deep: 15 %), *Rhizosolenia* (shallow: 9-21 %), and large
 427 centric diatoms (>20 μm) (shallow: 10-17 %; deep: 16-20 %), as well as the silicoflagellate *Dictyochoa*
 428 (shallow: 9-10 %; deep: 8 %), were also relatively high in terms of biovolume during period 1. During
 429 period 2, the community in terms of biovolume was quite mixed in terms of biovolume in the
 430 shallow trap (Figure 4B). The deep trap had, with similar contributions from *Fragilariopsis spp.* (22-
 431 28 %), *Dictyochoa* (14-15 %), *Coscinodiscus* (10 %), and, small (<20 μm, 9-14 %) and large (>20 μm, 9-
 432 19 %) centric diatoms in the deep trap during period 2. Since there has been little known work on the
 433 $\delta^{30}\text{Si}$ of *Dictyochoa* or indeed other silicoflagellates, we are not able to constrain the impact of this
 434 organism on our measured values. However, since the contribution by abundance was <5 % and
 435 diatoms were dominant (>85 %), their isotopic signature would need to be vastly different from that
 436 of diatoms to have an appreciable impact on our results.



438 **Figure 4: Phytoplankton assemblage of A,B) shallow and C, D) deep sediment trap samples,**
 439 **according to abundance (A, C) and biovolume (B, D). Plots A and C show phytoplankton**
 440 **contributing >5 % by abundance, and plots B and D show >5 % by biovolume. Other refers to all**
 441 **other counted taxa combined. Four samples were identified taxonomically for each trap. Green**
 442 **shading highlights productive period 1 and 2, as per figure 2. Note that only intact cells were**
 443 **counted.**

444

445 4. Discussion

446 In this study we measure the seasonal cycle of POC, PN and BSi fluxes as well as the $\delta^{13}\text{C}_{\text{POC}}$, $\delta^{15}\text{N}_{\text{PN}}$
447 and $\delta^{30}\text{Si}_{\text{BSi}}$ values of sinking particles collected in shallow (400 m) and deep (2000 m) sediment traps
448 in the Scotia Sea, Southern Ocean. Both the magnitude [of fluxes](#) and isotopic compositions were
449 generally similar in the shallow and deep sediment traps, suggesting that most remineralisation
450 occurred in the upper 400 m. This highlights that material reaching 400 m likely facilitates the
451 transfer of carbon much deeper in the ocean, sequestering carbon for longer time periods (Kwon et
452 al., 2009).

453 4.1. Seasonal flux cycles

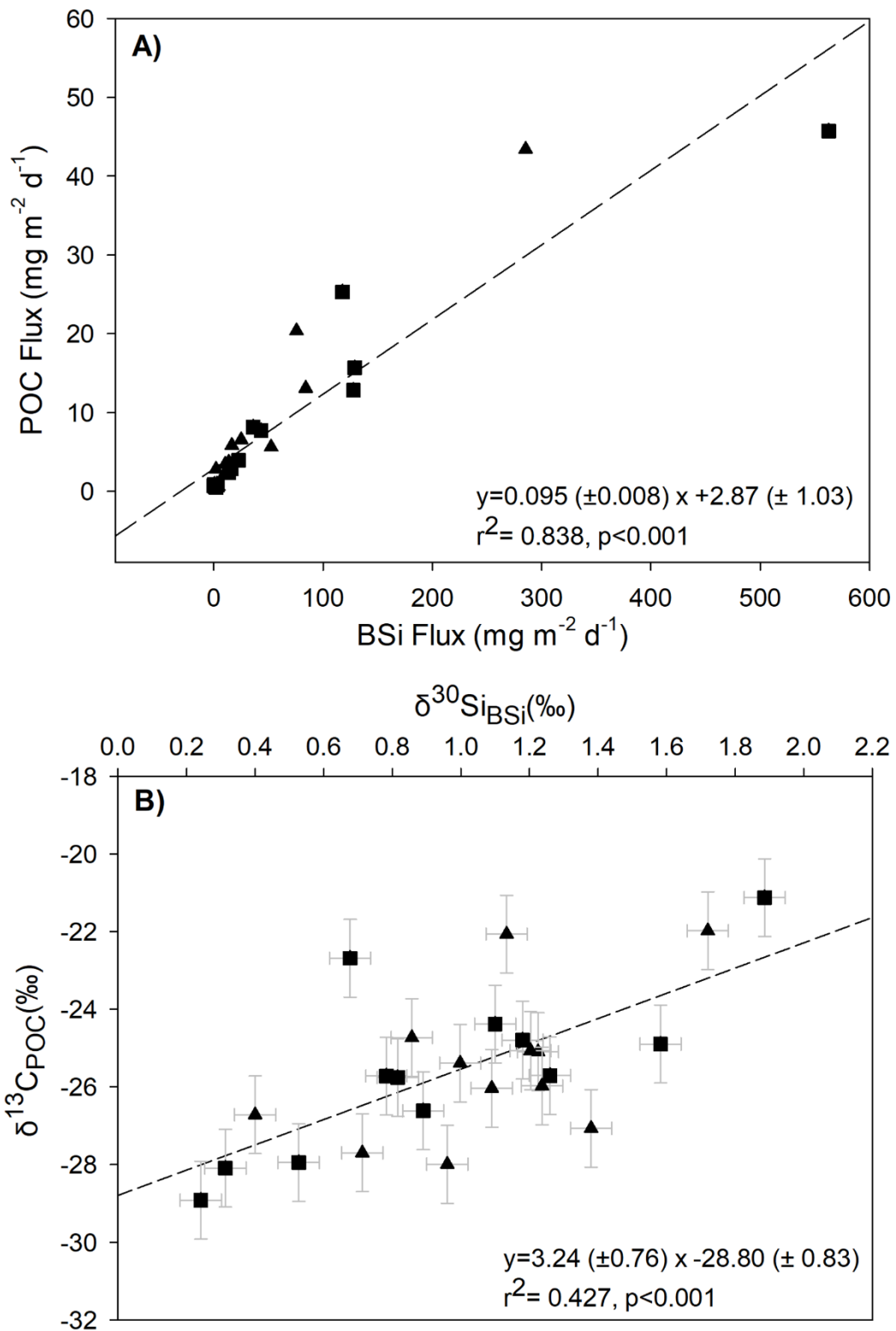
454 The seasonal cycles of POC agree well with previously published work at the same location (Manno
455 et al., 2015), with peaks in austral spring and late summer, though the peak POC fluxes recorded
456 here (45.7 mg C m⁻² d⁻¹ and 43.4 mg C m⁻² d⁻¹, in shallow and deep traps respectively) are higher than
457 those observed in previous years (22.9 mg C m⁻² d⁻¹; Manno et al., 2015). A smaller additional peak in
458 POC flux (<10 mg C m⁻² d⁻¹) occurred in April/May, in agreement with some previous years (Manno et
459 al., 2015). PN fluxes followed the same seasonal trend as POC for both deep and shallow traps
460 suggesting a similar source. The similar magnitude of POC:PN ratios in period 1 in the two traps
461 support consistency in the degree of degradation at these depths. The lower POC:PN ratios
462 measured in the deep trap between August and October, compared to the shallow trap are
463 consistent with a divergence in $\delta^{15}\text{N}_{\text{PN}}$ ratios, and could [indicate that material arriving at the two
464 traps is not necessarily sourced from the same region and time period in surface waters. Given the
465 slower sinking speeds at this low-productivity time of year, it is possible that material reaching the
466 deep trap is sourced from upstream of where material reaching the shallow trap is sourced in the
467 regional circulation system. Different source regions are likely characterised by different
468 phytoplankton assemblages with different nutrient stoichiometry, and the time taken for source
469 material to reach each of the traps may well lead to differences in degradation state of organic
470 matter, which could also lead to variations in POC:PN.](#)~~relate to a change in source material and/or
471 degradation state between the two traps at this time.~~

472 Our measured fluxes of BSi are higher than previously observed at this site at 2000 m ~~in 2012~~
473 (Rembauville et al., 2016). Maximum fluxes of 46.0 mg SiO₂ m⁻² d⁻¹ were recorded by Rembauville et
474 al. (2016) in January 2012, which though of similar magnitude to our summer peak of 84.3 mg SiO₂
475 m⁻² d⁻¹, is an order of magnitude lower than the spring peak of 285.4 mg SiO₂ m⁻² d⁻¹ in December
476 2018. However, the Rembauville et al. (2016) record ends in November and therefore would not
477 have captured the main peak in particle flux following the phytoplankton spring bloom in December
478 (apparent in satellite surface chlorophyll_a; Figure 2 in Rembauville et al. (2016)). Additionally, we do
479 not capture the first 3 weeks of January in our data. [Interannual variability in export flux can be high
480 due to the complexity of processes controlling the magnitude of export flux, such as community
481 structure, nutrient limitation and zooplankton activity.](#) Closset et al. (2015) measured very high
482 fluxes (>700 mg SiO₂ m⁻² d⁻¹) of BSi south of the ~~Sub-Antarctic Polar~~ Front in the Australian sector of
483 the Southern Ocean at 2000 m, and similarly high fluxes have been observed in other sectors
484 (Fischer et al., 2002; Honjo et al., 2000). [A study by Trull et al. \(2001\) measured fluxes of BSi in the
485 range of 30- 160 mg SiO₂ m⁻² d⁻¹ during the productive season in the same region as Closset et al.
486 \(2015\), again highlighting the high interannual variability.](#)

487 We define two main productive periods; productive period 1 from January to the start of April 2018,
488 and productive period 2 from September to the end of December 2018, when chlorophyll
489 concentrations were $>0.4 \text{ mg m}^{-3}$. Satellite data suggest the magnitude of chlorophyll concentration
490 was similar during both productive periods, but increasing in magnitude throughout period 2, and
491 decreasing in period 1, consistent with timing of sampling. The particle fluxes associated with
492 productive period 2 were much higher than those during productive period 1; a difference
493 that which is particularly pronounced for BSi fluxes. The bloom during period 2 was more
494 geographically widespread (Figure S2) and thus it is possible that if more of the material reaching the
495 trap was sourced from productive waters, this could have supported the higher fluxes observed at
496 this time. The observed higher BSi fluxes in productive period 2 could also relate to the presence of
497 more heavily silicified diatom species at this time, including the occurrence of resting spores
498 (*Chaetoceros* spp.; Figure 4, and Rembauville et al. (2016)), increased aggregation (and thus sinking)
499 potential, higher sinking rates, and/or reduced grazing pressure. The fact that we observed resting
500 spores at the end of productive period 2, suggests that nutrients may have started to become
501 limiting for at least some of the phytoplankton community (e.g. silicic acid and/or iron; Rembauville
502 et al., 2016). POC and BSi fluxes track each other closely and ratios suggest high-substantial export of
503 biogenic silica (Figure 5). This, combined with our visual observations of a dominance of
504 phytoplankton algal-material in the trap during the spring peak that was dominated by diatoms
505 (Figure 4), suggest an important role for diatoms in transferring organic carbon to the deep ocean at
506 this time. This could be achieved if cells are large, through large mineral (silica) ballasted cells sinking
507 at high velocities (Baumann et al., 2022), or through the bioprotection of internal organic matter
508 from grazing and oxidation by the diatom silica frustules (Passow and De La Rocha, 2006; Armstrong
509 et al., 2001; Smetacek et al., 2004).

510 4.2. Seasonal variations in isotope ratios

511 ~~In terms of the seasonality, we see broadly similar trends for both $\delta^{13}\text{C}_{\text{POC}}$ and $\delta^{30}\text{Si}_{\text{BSi}}$ (linear~~
512 ~~regression, $R^2 = 0.452$, $p < 0.001$, Figure 5), again highlighting the close coupling of carbon and silicon~~
513 ~~cycling processes. Despite the strong relationship between particulate fluxes of POC and BSi, the~~
514 ~~relationship between the $\delta^{13}\text{C}_{\text{POC}}$ and $\delta^{30}\text{Si}_{\text{BSi}}$ isotope signatures is less pronounced (significant but~~
515 ~~low R^2 ; linear regression; $R^2 = 0.42752$, $p < 0.001$; Figure 5). This may relate to greater variation in~~
516 ~~the fractionation factor for $\delta^{13}\text{C}$ compared to $\delta^{30}\text{Si}$ (Brandenburg et al., 2022), as well as differences~~
517 ~~in remineralisation of organic carbon and silicon in the frustule. Additionally, whereas most of the~~
518 ~~$\delta^{30}\text{Si}$ signal is from diatoms, the $\delta^{13}\text{C}$ signal in the sediment trap material is also impacted by the~~
519 ~~presence of other organic material, e.g. zooplankton faecal pellets. We do not find significant~~
520 ~~relationships between $\delta^{15}\text{N}_{\text{PN}}$ and $\delta^{13}\text{C}_{\text{POC}}$ ($r^2 = 0.00$, $p = 0.63$) or $\delta^{30}\text{Si}_{\text{BSi}}$ ($r^2 = 0.00$, $p = 0.60$). We~~
521 ~~discuss results for each of the break-the-season-into-3 main periods for discussion, productive period~~
522 ~~1 (first export event), the winter flux hiatus, and productive period 2 (second export event).~~



523

524 **Figure 5: Relationship between BSi and POC for data from both deep (triangles) and shallow**
 525 **(squares) sediment traps. A) Regression between BSi and POC fluxes, and B) between $\delta^{13}\text{C}_{\text{POC}}$ and**
 526 **$\delta^{30}\text{Si}_{\text{BSi}}$. Regression lines are shown by dotted lines with coefficients and associated standard errors**
 527 **also shown. *Error bars on isotope values represent the maximum error on sediment trap $\delta^{13}\text{C}_{\text{POC}}$***

528 (±1 ‰) associated with formaldehyde preservation (Mincks et al., 2008) and for $\delta^{30}\text{Si}_{\text{BSi}}$, the scaled
529 error bar represents 2 x SD (‰-0.07 ‰) for the analytical sample replicates.

531 4.2.1. Productive period 1

533 During productive period 1, $\delta^{13}\text{C}_{\text{POC}}$ is low, averaging -28.5930 and -27.2452 ‰ in shallow and deep
534 traps respectively, close to that expected for Southern Ocean phytoplankton employing typical C3
535 metabolism (i.e. diffusive CO_2 transfer into the internal cell pool and Rubisco carboxylation) (Raven,
536 1997). This is consistent with the dominance of diatoms (*Fragilariopsis spp.*) in the trap material, as
537 Bacillariophyceae are known to employ C3 metabolism (Table IV in Raven, 1997). Preferential uptake
538 of ^{28}Si by diatoms (De La Rocha et al., 1997) during the late spring bloom of productive period 1 also
539 explains the low $\delta^{30}\text{Si}_{\text{BSi}}$ values. BSi:POC ratios were elevated at the start of productive period 1,
540 which may suggesting that phytoplankton were heavily silicified. The contribution of non-siliceous
541 phytoplankton was low during the periods analysed for phytoplankton composition (<2%, with the
542 exception of the shallow trap in the late January sample where the contribution was 6.7%), though
543 we cannot rule out higher contributions of non-siliceous phytoplankton during other periods which
544 could account forive the lower BSi:POC ratios at these times. After initial low values, we see a
545 progressive increase in both $\delta^{13}\text{C}_{\text{POC}}$ and $\delta^{30}\text{Si}_{\text{BSi}}$, reflecting the progressive utilisation of both ^{12}C and
546 ^{28}Si as nutrient pools are consumed during the bloom. As such, the diatom cells reaching the
547 sediment trap in late spring/summer were utilising increasingly isotopically-enriched C and Si for
548 growth leading to progressive isotopic enrichment of the cells sinking into the sediment trap. This
549 observation fits with elevated but decreasing surface chlorophyll concentrations from February to
550 April 2018. Increasing $\delta^{13}\text{C}_{\text{POC}}$ and $\delta^{30}\text{Si}_{\text{BSi}}$ into the late summer may also partially reflect preferential
551 remineralisation of the more labile ^{12}C and ^{28}Si in particles as they sink through the upper 400 m of
552 the water column. The lack of variation in $\delta^{13}\text{C}_{\text{POC}}$ and $\delta^{30}\text{Si}_{\text{BSi}}$ between 400 and 2000 m in our study
553 suggests that remineralisationthis may be limited over-between these depth-ranges, or that there is
554 no further fractionation effect. Whilst laboratory-based silica dissolution experiments are equivocal
555 (Demarest et al., 2009; Wetzel et al., 2014), our findings agree with field studies that also indicate a
556 lack of Si isotopic fractionation during diatom silica dissolution (Closset et al., 2015; Egan et al.,
557 2012).

558 During productive period 1 there was no clear trend in $\delta^{15}\text{N}_{\text{PN}}$, with values between -1.95 and +2.96
559 ‰. We speculate that this mixed signal with no significant difference between deep and shallow
560 traps-resulted from a combination of surface phytoplankton using both ammonium and nitrate as
561 the inorganic nitrogen source, and variability in the sediment trap material composition.
562 Enrichments of 2-4 ‰ occur between successive trophic levels, and egestion and excretion can have
563 varying isotopic effects (see Section 4.3), thus the presence of faecal pellets, animal moults and
564 carcasses could alter the isotopic composition of the sediment trap material. Additionally, any supply
565 of ammonium through remineralisation would be utilised quickly because ammonium is kinetically
566 favourable to nitrate (Glibert et al., 2016), resulting in particles with a decreased $\delta^{15}\text{N}_{\text{PN}}$ compared to
567 those produced by nitrate assimilation.

569 4.2.2. Winter hiatus

570 Between May and August, both $\delta^{13}\text{C}_{\text{POC}}$ and $\delta^{30}\text{Si}_{\text{BSi}}$ showed little change, with a slight progressive
571 decrease for $\delta^{13}\text{C}_{\text{POC}}$ and ~~slight~~ increase in $\delta^{30}\text{Si}_{\text{BSi}}$. It is possible that the slight progressive trend
572 towards a lighter carbon isotopic composition of sinking particles from -24.94 to -25.98 ‰ is driven
573 by a mixture of older, isotopically heavier particles that have undergone partial remineralisation and
574 the input of material of different isotopic composition from the small secondary peak in POC we
575 observed in April/May. An input of smaller, more slowly sinking cells reaching the trap in increasing
576 numbers following the initial late spring peak in production could drive the lower $\delta^{13}\text{C}_{\text{POC}}$ at this time.
577 Additionally, the pulse of material could be driven by a successive peak in production of a different
578 phytoplankton community with a different isotopic signature. Korb et al. (2012) found an increasing
579 presence of dinoflagellates from spring to summer, as well as seasonal changes in the size structure
580 of the phytoplankton community to the northwest of South Georgia, supporting either hypothesis.
581 We do not have the species composition data from this time period to evidence this directly, but we
582 suggest that the reduction in $\delta^{13}\text{C}_{\text{POC}}$ does not relate to a mixing event and a resupply of ^{12}C , due to
583 the fact that $\delta^{30}\text{Si}_{\text{BSi}}$ continued to increase slowly. Given the generally lighter silicon isotopic
584 composition of seawater below the photic zone, we would expect a mixing event to also result in a
585 decline in seawater $\delta^{30}\text{Si}$ and consequently $\delta^{30}\text{Si}_{\text{BSi}}$. This would mean that our hypothesised shift in
586 phytoplankton species composition in the traps (May-August) did not impact Si fractionation to the
587 same extent as carbon isotopes. Whereas size, growth rates, cell geometry and different carbon
588 acquisition mechanisms have all been highlighted as impacting the $\delta^{13}\text{C}_{\text{POC}}$ of marine plankton (Popp
589 et al., 1999, 1998; Bidigare et al., 1999; Trull and Armand, 2001; Tuerena et al., 2019), species-
590 dependent Si fractionation by polar and subpolar diatoms has only been observed in the laboratory,
591 not in the field (Annett et al., 2017; Cassarino et al., 2017; Sutton et al., 2013). $\delta^{15}\text{N}_{\text{PN}}$ in the shallow
592 trap showed a slight progressive decrease ~~over the winter period~~ from April to July, before increasing
593 in August to 5.42 ‰. The progressive decrease is consistent with the propagation of the surface
594 signal of phytoplankton growth and fractionation, with a longer time lag than during spring and
595 summer due to slower sinking rates during the low-productivity period. Decreasing $\delta^{15}\text{N}_{\text{PN}}$ reflects
596 the increasing influence of ammonium uptake, either in the same locale or upstream in the regional
597 circulation system, which leads to lower $\delta^{15}\text{N}_{\text{PN}}$ than nitrate uptake in the slowly-sinking flux, with
598 increasing influence of ammonium uptake as the season progresses that leads to low $\delta^{15}\text{N}_{\text{PN}}$. The
599 large range in $\delta^{15}\text{N}_{\text{PN}}$ in the deep trap in July makes it difficult to determine with certainty a trend in
600 $\delta^{15}\text{N}_{\text{PN}}$ in the deep trap between July and October. Dissimilar trends in $\delta^{15}\text{N}_{\text{PN}}$ between the two traps
601 over the winter period also support the argument that material reaching these two traps may have a
602 different source region or time period in surface waters (Section 4.1).

603

604 4.2.3. Productive period 2

605 At the start of productive period 2 (September) we saw a significant decrease in $\delta^{30}\text{Si}_{\text{BSi}}$ (~0.5 ‰) in
606 both traps suggesting resupply of ^{28}Si enriched silicic acid to the euphotic zone via mixing.
607 Interestingly, we did not see the same consistent shift in carbon isotopes; we measured a ~1 ‰
608 decrease in the shallow trap $\delta^{13}\text{C}_{\text{POC}}$ and a ~1 ‰ increase in the deep trap $\delta^{13}\text{C}_{\text{POC}}$. We speculate that
609 this mixing could bring waters of increased silicic acid concentrations to the surface, promoting full
610 expression of the isotope fractionation effect from phytoplankton uptake and thus lower $\delta^{30}\text{Si}_{\text{BSi}}$ in
611 sinking particles. To match our observations, these mixed waters would need to be similar in
612 dissolved inorganic carbon concentrations and $\delta^{13}\text{C}$, which could relate to the depth of mixing and

613 differences in the depth at which POC and BSi are remineralised (Friedrich and Rutgers van der Loeff,
614 2002; Weir et al., 2020). We note that current velocities recorded at this time were elevated (Figure
615 S1), particularly in the deep trap, suggesting a shift in the surrounding velocity fields, which may
616 have resulted in biased sample collection at this time through either over- or under-collection
617 (Buesseler et al., 2007). Whereas $\delta^{13}\text{C}_{\text{POC}}$ progressively increased during productive period 2, from -
618 25.88 ‰ in September to -21.56 ‰ at the end of December (mean of deep and shallow traps),
619 $\delta^{30}\text{Si}_{\text{BSi}}$ continued to decrease until November before showing a sudden increase from +0.74 ‰ to
620 +1.80 ‰ at the end of the sampling period. This may suggest that DSi, or co-limiting nutrients, was
621 replete, and uptake could occur unhindered until November 2018 when very high rates of
622 production and the associated high fluxes of BSi increased the demand for DSi and led to enrichment
623 of $\delta^{30}\text{Si}$ in overlying waters and subsequently sinking siliceous phytoplankton. For carbon, uptake
624 was sufficient from September to progressively deplete source waters in ^{12}C , driving an increase in
625 $\delta^{13}\text{C}$ in surface waters and newly formed phytoplankton cells. BSi:POC ratios increased from
626 September to December suggesting that material reaching the traps was increasingly silicified.

627 Interestingly, unlike C and Si isotopes, we saw a divergence in the nitrogen isotopic composition of
628 deep and shallow traps between August and December. The sharp increase in mean $\delta^{15}\text{N}_{\text{PN}}$ from
629 +1.32 ‰ in July to +5.42 ‰ in August 2018 in the shallow trap that initiated the divergence strongly
630 suggests an advective change in source material. As noted above, this was a period of increased
631 horizontal velocities and may have facilitated material reaching the two traps from different sources
632 of differing initial composition and degradation states. The substantially lower $\delta^{15}\text{N}_{\text{PN}}$ in the deep
633 trap from August to November, compared to that of the shallow trap is surprising. It would be
634 expected, that, as particles sink and are progressively decomposed this would remove dissolved
635 nitrogen depleted in ^{15}N , thus increasing $\delta^{15}\text{N}_{\text{PN}}$ in the particles. Indeed many studies have observed
636 this trend of increasing $\delta^{15}\text{N}$ with depth in suspended particles (Altabet et al., 1991 and references
637 therein). However, like Altabet et al. (1991), we observe lower $\delta^{15}\text{N}_{\text{PN}}$ in sinking particles in the deep
638 sediment trap. This has also been observed previously in Antarctic waters (Wada et al., 1987).
639 Though the reason for this is not well understood (Sigman and Fripiat, 2019), it appears to be a
640 consistent phenomenon. Particles in our deep trap must therefore be gaining light nitrogen or losing
641 heavy nitrogen and could reflect a different source composition. In agreement with Altabet et al.
642 (1991), we suggest that lateral transport of low $\delta^{15}\text{N}_{\text{PN}}$ from a region of increased ammonium-based
643 production could explain this, highlighting a difference in the source of sinking particles to the two
644 traps. Altabet et al. (1991) also suggests that, since protein nitrogen is 3 ‰ higher than bulk
645 nitrogen, the selective decomposition of protein could explain the decrease in $\delta^{15}\text{N}$ with depth,
646 though why this would not be the case also for suspended PN is unclear. We observe the greatest
647 divergence in shallow and deep N isotope compositions during periods of low PN flux (Figure 3),
648 consistent with the observations of Altabet et al. (1991), enabling a low flux of laterally supplied
649 material to have an amplified impact on the isotope signal. In support of this, in December when
650 particle fluxes increase sharply with the spring bloom, $\delta^{15}\text{N}_{\text{PN}}$ in the deep trap increases more in line
651 with that of the shallow trap, highlighting a switch from source material being dominated by lateral
652 supply when vertical supply is negligible, to the dominance of vertical supply from surface
653 production following the phytoplankton bloom.

654

655 4.3. Drivers of $\delta^{15}\text{N}$ shifting isotopic ratios

656 The mean flux-weighted isotopic composition measured during productive periods 1 (January to [the](#)
657 [start of](#) April 2018) and 2 (September to [the end of](#) December 2018) suggests that the processes
658 driving the flux of material at these times differ (Figure 3, Table 1). The divergence in the $\delta^{15}\text{N}_{\text{PN}}$ of
659 deep and shallow trap material during period 2 limits our ability to compare the temporal shifts in
660 mean isotopic ratios for nitrogen isotopes, so we focus here on $\delta^{13}\text{C}_{\text{POC}}$ and $\delta^{30}\text{Si}_{\text{BSi}}$. Since our record
661 does not extend beyond December 2018, and we do not capture the first 3 weeks of January 2018
662 when fluxes [we](#) are likely high, we do not record the initial value at this time, however, we would
663 expect $\delta^{13}\text{C}_{\text{POC}}$ to be even more negative at this time. We cannot determine if $\delta^{13}\text{C}_{\text{POC}}$ and $\delta^{30}\text{Si}_{\text{BSi}}$
664 would return to values akin to that in period 1 in the following late spring-summer season (January
665 2019). We saw a shift in $\delta^{13}\text{C}_{\text{POC}}$ from a mean of -28.31 ‰ in January 2018 at the time of our first
666 measurements to -25.88 ‰ in September at the start of period 2. This coincided with a change in
667 community structure, with abundance dominated by *Fragilariopsis spp.* in period 1 to a more mixed
668 community in period 2. Of the abundant phytoplankton species (>5%, Figure 4A, C), we find
669 statistically significant linear relationships between $\delta^{13}\text{C}_{\text{POC}}$ and percent abundance for *Fragilariopsis*
670 *spp.* (empty: $R^2 = 0.926$, $p < 0.001$), *Thalassionema nitzschioides* (live: $R^2 = 0.774$, $p = 0.004$; empty: $R^2 =$
671 0.844 , $p = 0.001$), and *Chaetoceros spp. (resting spore)* ($R^2 = 0.732$, $p = 0.007$). We stress this is based
672 on only 8 samples. Nevertheless, these robust samples show that there was a shift in phytoplankton
673 community structure. Though *Fragilariopsis spp.* were mainly empty cells, colonisation by bacteria
674 (Grossart et al., 2003; Kjørboe et al., 2003) may facilitate carbon transfer within and on these cells,
675 and certainly the live cells of *T. nitzschioides* and resting spores of *Chaetoceros spp.* would act as
676 agents of carbon transfer (Agusti et al., 2015; Salter et al., 2012; Rembauville et al., 2016).

677 We examine whether this shift in phytoplankton community composition is associated with a change
678 in SA:V (Table 2) since greater fractionation of carbon in smaller phytoplankton cells with higher
679 SA:V is well observed in the literature (e.g. Popp et al., 1998; Tuerena et al., 2019). There was a
680 statistically significant (paired t-test, $p = 0.008$) difference in the community SA:V between productive
681 periods, increasing from $0.35 \mu\text{m}^2 \mu\text{m}^{-3}$ in period 1 to $0.51 \mu\text{m}^2 \mu\text{m}^{-3}$ in period 2. However, this would
682 result in increased isotopic fractionation during period 2, [in opposition which is the opposite](#) to what
683 we observed. We note here, that as only intact cells were counted, the measured SA:V ratios may
684 not fully account for the isotopic composition of the trap material due to the presence of
685 fragmented material. It is possible that there was a change in the mechanism of carbon uptake with
686 the more mixed phytoplankton community in period 2 using HCO_3^- instead of CO_2 or employing
687 carbon concentrating mechanisms (CCMs), both of which would result in higher $\delta^{13}\text{C}_{\text{POC}}$ than the
688 diffusive uptake of CO_2 [and via](#) Rubisco [carboxylation](#) (Raven, 1997; Cassar et al., 2004). Studies show
689 that there is much diversity amongst diatoms in the use of CCMs and many are able to take up both
690 CO_2 and HCO_3^- (Trimborn et al., 2009; Roberts et al., 2007; Shen et al., 2017; Young et al., 2016). We
691 suggest that species--driven differences in carbon uptake mechanisms account in part for the
692 differing $\delta^{13}\text{C}_{\text{POC}}$ that we observed during the two main productive periods.

693 **Table 2: Phytoplankton cell community surface area to volume (SA:V) ratios measured in deep and**
694 **shallow sediment traps for samples enumerated in both productive periods 1 and 2.**

Bottle open date	Depth	Period	Mean community SA:V
25/01/2018	Shallow	1	0.39
01/02/2018	Shallow	1	0.35

01/02/2018	Deep	1	0.33
15/02/2018	Deep	1	0.32
01/12/2018	Deep	2	0.53
01/12/2018	Shallow	2	0.48
15/12/2018	Deep	2	0.53
15/12/2018	Shallow	2	0.52

695

696 We also observed a shift in the mean flux-weighted $\delta^{30}\text{Si}_{\text{BSi}}$ ratios (Table 1) between period 1 and
697 period 2. With the exception of one culture study (Sutton et al., 2013), systematic species-driven
698 shifts in $\delta^{30}\text{Si}_{\text{BSi}}$ fractionation have not been observed (e.g., De La Rocha et al., 1997), suggesting that
699 there may be an additional driver of the changing isotopic ratios. Since, prior to our first
700 measurements there had been a long-lasting phytoplankton bloom (Figure S2), we would expect
701 production to have utilised much of the light ^{28}Si , resulting in particles with enriched $\delta^{30}\text{Si}_{\text{BSi}}$ reaching
702 the trap in January 2018. However, we observe isotopically light mean values of +0.48 ‰ at the start
703 of sampling at the end of January, suggesting that there must have been a resupply of ^{28}Si . Physical
704 mixing, bringing deep and benthic waters rich in nutrients, including iron, to the surface waters
705 around South Georgia, are known to support the large blooms occurring downstream of South
706 Georgia (Matano et al., 2020; Nielsdóttir et al., 2012) and could supply both ^{12}C -enriched dissolved
707 inorganic carbon and ^{28}Si -enriched silicic acid. Additional nutrients could also be supplied to our
708 study region by glacial discharge associated with isotopically light silicon isotopic signatures (Matano
709 et al., 2020; Hatton et al., 2019), or benthic fluxes from shelf sediments, likely also releasing
710 isotopically light DSi (Ng et al., 2020; Cassarino et al., 2020; Closset et al., 2022). Therefore, we
711 suggest that low values (increased fractionation) of $\delta^{13}\text{C}_{\text{POC}}$ and $\delta^{30}\text{Si}_{\text{BSi}}$ during period 1 relate to
712 increased nutrient availability enabling full expression of the isotopic fractionation and thus
713 isotopically light particulate material to reach the sediment trap.

714 The ocean circulation in our study region is complex and variable on fine spatial and temporal scales,
715 affecting horizontal and vertical velocities (e.g. Boehme et al., 2008). It is clear from the currents
716 measured at the depths of our two traps (Figure S1), that both the direction and magnitude of the
717 flow can vary within and between seasons and is not necessarily consistent between the two depths.
718 There are thus potentially different source regions for material in the two traps at certain times of
719 the year [as suggested for example by \$\delta^{15}\text{N}_{\text{PN}}\$ ratios in winter](#). We lack the full depth resolution of
720 vertical and horizontal velocity fields and information on sinking rates to confirm this, but previous
721 studies have highlighted variability in the locations of the Southern Antarctic Circumpolar Current
722 Front and the Polar Front, as well as eddies generated from these fronts, in our study region (Moore
723 et al., 1999; Boehme et al., 2008; Whitehouse et al., 1996). We suggest that variability in ocean
724 current velocities could explain different isotopic ratios in period 1 and 2, through the supply of
725 material to the traps from different source regions with differing nutrient and remineralisation
726 regimes. Different source waters would impact nutrient availability including iron supply, uptake and
727 recycling (Hawco et al., 2021; Ellwood et al., 2020), which in turn influences species composition,
728 nutrient utilisation and uptake rates (e.g. Meyerink et al., 2019). This highlights the importance of
729 making synchronous, and full depth resolution measurements of, physical processes such as current
730 strength and direction, to be able to distinguish between spatial and temporal drivers of shifts in
731 species composition, particle flux and isotopic composition.

732 Since trophic transfer is known to impact both carbon and nitrogen isotope compositions of organic
733 matter, the presence of moults and faecal pellets in trap samples ~~are-is~~ also important to consider.
734 An incubation study focussed on *Euphausia superba* found that the $\delta^{15}\text{N}$ of the *E. superba* faecal
735 pellets was always lower than that of the copepods they ingested, though still higher than that of
736 POM (Schmidt et al., 2003). Additionally, Tamelander et al. (2006) measured faecal pellets produced
737 by copepods with depleted ^{15}N compared to the algal food source. Though a few studies on
738 temperate and subtropical copepods showed that the faecal material had similar or slightly higher
739 $\delta^{15}\text{N}$ than the food source (Altabet and Small, 1990; Checkley and Entzeroth, 1985), there is not a
740 consistent fractionation effect of egestion, for either $\delta^{15}\text{N}$ or $\delta^{13}\text{C}$, which may relate to compositional
741 differences (protein, carbohydrate, lipid) and their isotopic values (Tamelander et al., 2006). We are
742 therefore not able to determine the impact of faecal pellets or moults on the isotopic composition of
743 our samples. As phytoplankton material dominated at the times of peak flux, we suggest that the
744 importance of faecal pellets and moults may be greater during periods of lower flux, however we
745 cannot rule out their contribution during the bloom periods. We suggest that it would be highly
746 informative to conduct particle specific isotope analysis of common particle types in sediment traps,
747 such as faecal pellets, phytoplankton detritus and zooplankton moults, to improve our ability to
748 determine the impact of particle flux composition on bulk isotope compositions.

749

750 **Conclusion**

751 The seasonal cycles in primary productivity and nutrient uptake in surface waters at our study site in
752 the Scotia Sea are reflected in the fluxes and isotopic ratios of sinking particulate material. We find
753 that most remineralisation occurs in the upper 400 m of the water column and below this the
754 magnitude of the flux of sinking material is relatively consistent, supported by consistency in
755 POC:PON ratios. We find that particulate fluxes of C_7 and BSi are tightly coupled which highlights the
756 importance of siliceous material in the transfer of POC to depth. We suggest that a change in
757 phytoplankton community structure can at least partly explain the shifts in carbon isotopic
758 composition between the two productive periods measured here. Though complex, seasonal
759 patterns in isotopic composition of particulate material reaching the sediment traps do reflect the
760 degree and type of nutrient utilisation in the source surface waters. Our data also suggests an
761 importance of laterally supplied material to the sediment traps and supports seasonal differences in
762 source regions. Our results highlights ~~the need for how, through~~ more detailed mechanistic
763 understanding of the drivers of POC flux, and biogeochemical cycling, ~~to, we can~~ improve estimates
764 of the current and future strength of the biological carbon pump and the ocean's role as a CO_2 sink.

765

766 **Data availability**

767 Phytoplankton abundances and biovolume, as well as mean flux and isotopic ratios are available
768 with the following DOI's:

769 DOI in progress with the British Antarctic Survey Polar Data Centre

770 **Author contributions**

771 AB and CM conceived the study and participated in fieldwork to collect samples. AB conducted
772 laboratory analysis with support from TW, LF, and UD for isotope analysis. MW conducted
773 phytoplankton analysis and provided intellectual input on phytoplankton community composition.
774 SH and KH provided support for isotopic analysis and contributed to the interpretation of the data
775 and implications. CC supported uncertainty analysis. All authors contributed text to the manuscript.

776 **Competing Interests**

777 The authors declare that they have no conflict of interest.

778

779 **Acknowledgements**

780 We are very grateful to the scientists and crew aboard research cruises JR17002 and DY098 for their
781 efforts to deploy and recover the P3 mooring. We thank staff at the Bristol Isotope Group for
782 running and maintenance of the mass spectrometer facilities at the University of Bristol, as well as
783 Colin Chilcott for technical support for C and N analysis at the University of Edinburgh. AB and CM
784 were supported by NC-ALI funding and ecosystems programme. CM was also funded by UKRI FLF
785 project MR/T020962/1. SH was supported by the United Kingdom Natural Environment Research
786 Council through grant NE/K010034/1. UD was supported by the UK NERC through grant
787 NE/P006108/1. LF was supported by a NERC GW4+ DTP studentship and TW by a CSC-UoB Joint
788 Scholarship. We thank Sally Thorpe and Emma Young for insights on the physical oceanographic
789 conditions of the region. Finally, a special thanks to Flo Atherden for her dedicated work picking out
790 swimmers from the shallow sediment trap.

791

792 **References**

793 Agustí, S., González-Gordillo, J. I., Vaqué, D., Estrada, M., Cerezo, M. I., Salazar, G., Gasol, J. M., and
794 Duarte, C. M.: Ubiquitous healthy diatoms in the deep sea confirm deep carbon injection by the
795 biological pump, *Nat. Commun.*, 6, 1–8, <https://doi.org/10.1038/ncomms8608>, 2015.

796 Altabet, M. A. and Small, L. F.: Nitrogen isotopic ratios in fecal pellets produced by marine
797 Zooplankton, *Geochim. Cosmochim. Acta*, 54, 155–163, [https://doi.org/10.1016/0016-](https://doi.org/10.1016/0016-7037(90)90203-W)
798 [7037\(90\)90203-W](https://doi.org/10.1016/0016-7037(90)90203-W), 1990.

799 Altabet, M. A., Deuser, W. G., Honjo, S., and Stienen, C.: Seasonal and depth-related changes in the
800 source of sinking particles in the North Atlantic, *Nature*, 354, 136–139,
801 <https://doi.org/10.1038/354136a0>, 1991.

802 Annett, A. L., Henley, S. F., Venables, H. J., Meredith, M. P., Clarke, A., and Ganeshram, R. S.: Silica
803 cycling and isotopic composition in northern Marguerite Bay on the rapidly-warming western
804 Antarctic Peninsula, *Deep. Res. Part II Top. Stud. Oceanogr.*, 139, 132–142,
805 <https://doi.org/10.1016/j.dsr2.2016.09.006>, 2017.

806 Armstrong, R. A., Lee, C., Hedges, J. I., Honjo, S., and Wakeham, S. G.: A new, mechanistic model for
807 organic carbon fluxes in the ocean based on the quantitative association of POC with ballast
808 minerals, *Deep. Res. Part II Top. Stud. Oceanogr.*, 49, 219–236, [https://doi.org/10.1016/S0967-](https://doi.org/10.1016/S0967-0645(01)00101-1)
809 [0645\(01\)00101-1](https://doi.org/10.1016/S0967-0645(01)00101-1), 2001.

810 Baumann, M., Joy Paul, A., Taucher, J., Thomas Bach, L., Goldenberg, S., Stange, P., Minutolo, F.,

811 Riebesell, U., and Baumann mbaumann, M.: Drivers of Particle Sinking Velocities in the Peruvian
812 Upwelling System, EGU sphere. Prepr., 2022.

813 Belcher, A., Manno, C., Ward, P., Henson, S. A., Sanders, R., and Tarling, G. A.: Copepod faecal pellet
814 transfer through the meso- and bathypelagic layers in the Southern Ocean in spring, *Biogeosciences*,
815 14, <https://doi.org/10.5194/bg-14-1511-2017>, 2017.

816 Belcher, A., Manno, C., Thorpe, S., and Tarling, G.: Acantharian cysts: high flux occurrence in the
817 bathypelagic zone of the Scotia Sea, Southern Ocean, *Mar. Biol.*, 165,
818 <https://doi.org/10.1007/s00227-018-3376-1>, 2018.

819 Bidigare, R., Hanson, L., Buesseler, K. O., Wakeham, G., Freeman, H., Pancost, R. D., Millero, J.,
820 Steinberg, P., Popp, N., Latasa, M., Landry, R., and Laws, A.: Iron-stimulated changes in ^{13}C
821 fractionation and export by equatorial Pacific phytoplankton: Toward a paleogrowth rate proxy,
822 *Paleoceanography*, 14, 589–595, <https://doi.org/10.1029/1999PA900026>, 1999.

823 Boehme, L., Meredith, M. P., Thorpe, S. E., Biuw, M., and Fedak, M.: Antarctic circumpolar current
824 frontal system in the South Atlantic: Monitoring using merged Argo and animal-borne sensor data, *J.*
825 *Geophys. Res.*, 113, C09012, <https://doi.org/10.1029/2007JC004647>, 2008.

826 Brandenburg, K. M., Rost, B., Van De Waal, D. B., Hoins, M., and Sluijs, A.: Physiological control on
827 carbon isotope fractionation in marine phytoplankton, *Biogeosciences*, 19, 3305–3315,
828 <https://doi.org/10.5194/bg-19-3305-2022>, 2022.

829 Buesseler, K. O., Antia, A. N., Chen, M., Fowler, S. W., Gardner, W. D., Gustafsson, O., Harada, K.,
830 Michaels, A. F., Rutgers van der Loeff, M., Sarin, M., Steinberg, D. K., and Trull, T.: An assessment of
831 the use of sediment traps for estimating upper ocean particle fluxes, *J. Mar. Res.*, 65, 345–416,
832 <https://doi.org/10.1357/002224007781567621>, 2007.

833 Cardinal, D., Alleman, L. Y., De Jong, J., Ziegler, K., and Andre, L.: Isotopic composition of silicon
834 measured by multicollector plasma source mass spectrometry in dry plasma mode, *J. Anal. At.*
835 *Spectrom.*, 18, 213–218, <https://doi.org/10.1039/b210109b>, 2003.

836 Cassar, N., Laws, E. A., Bidigare, R. R., and Popp, B. N.: Bicarbonate uptake by Southern Ocean
837 phytoplankton, *Global Biogeochem. Cycles*, 18, 1–10, <https://doi.org/10.1029/2003GB002116>, 2004.

838 Cassarino, L., Hendry, K. R., Meredith, M. P., Venables, H. J., and De La Rocha, C. L.: Silicon isotope
839 and silicic acid uptake in surface waters of Marguerite Bay, West Antarctic Peninsula, *Deep. Res. Part*
840 *II Top. Stud. Oceanogr.*, 139, 143–150, <https://doi.org/10.1016/j.dsr2.2016.11.002>, 2017.

841 Cassarino, L., Hendry, K., Henley, S. F., Macdonald, E., Arndt, S., Freitas, F. S., Pike, J., and Firing, Y. L.:
842 Sedimentary Nutrient Supply in Productive Hot Spots off the West Antarctic Peninsula Revealed by
843 Silicon Isotopes, *Global Biogeochem. Cycles*, <https://doi.org/10.1029/2019GB006486>, 2020.

844 Checkley, D. M. and Entzeroth, L. C.: Elemental and isotopic fractionation of carbon and nitrogen by
845 marine, planktonic copepods and implications to the marine nitrogen cycle, *J. Plankton Res.*, 7, 553–
846 568, <https://doi.org/https://doi.org/10.1093/plankt/7.4.553>, 1985.

847 Closset, I., Cardinal, D., Bray, S. G., Thil, F., Djouaev, I., Rigual-Hernández, A. S., and Trull, T. W.:
848 Seasonal variations, origin, and fate of settling diatoms in the Southern Ocean tracked by silicon
849 isotope records in deep sediment traps, *Global Biogeochem. Cycles*, 29, 1495–1510,
850 <https://doi.org/10.1002/2015GB005180>, 2015.

851 Closset, I., Brzezinski, M. A., Cardinal, D., Dapoigny, A., Jones, J. L., and Robinson, R.: A silicon
852 isotopic perspective on the contribution of diagenesis to the sedimentary silicon budget in the
853 Southern Ocean, *Geochim. Cosmochim. Acta*, 327, 298–313, 2022.

854 Conley, D. J.: An interlaboratory comparison for the measurement of biogenic silica in sediments,
855 *Mar. Chem.*, 63, 39–48, [https://doi.org/10.1016/S0304-4203\(98\)00049-8](https://doi.org/10.1016/S0304-4203(98)00049-8), 1998.

856 Demarest, M. S., Brzezinski, M. A., and Beucher, C. P.: Fractionation of silicon isotopes during
857 biogenic silica dissolution, *Geochim. Cosmochim. Acta*, 73, 5572–5583,
858 <https://doi.org/10.1016/j.gca.2009.06.019>, 2009.

859 DeVries, T.: Atmospheric CO₂ and Sea Surface Temperature Variability Cannot Explain Recent
860 Decadal Variability of the Ocean CO₂ Sink, *Geophys. Res. Lett.*, 49, 1–17,
861 <https://doi.org/10.1029/2021GL096018>, 2022.

862 Egan, K. E., Rickaby, R. E. M., Leng, M. J., Hendry, K. R., Hermoso, M., Sloane, H. J., Bostock, H., and
863 Halliday, A. N.: Diatom silicon isotopes as a proxy for silicic acid utilisation: A Southern Ocean core
864 top calibration, *Geochim. Cosmochim. Acta*, 96, 174–192,
865 <https://doi.org/10.1016/j.gca.2012.08.002>, 2012.

866 Ellwood, M. J., Strzpek, R. F., Strutton, P. G., Trull, T. W., Fourquez, M., and Boyd, P. W.: Distinct
867 iron cycling in a Southern Ocean eddy, *Nat. Commun.*, 11, 1–8, [https://doi.org/10.1038/s41467-020-](https://doi.org/10.1038/s41467-020-14464-0)
868 [14464-0](https://doi.org/10.1038/s41467-020-14464-0), 2020.

869 Fischer, G., Gersonde, R., and Wefer, G.: Organic carbon, biogenic silica and diatom fluxes in the
870 marginal winter sea-ice zone and in the Polar Front Region: Interannual variations and differences in
871 composition, *Deep. Res. Part II Top. Stud. Oceanogr.*, 49, 1721–1745,
872 [https://doi.org/10.1016/S0967-0645\(02\)00009-7](https://doi.org/10.1016/S0967-0645(02)00009-7), 2002.

873 Friedrich, J. and Rutgers van der Loeff, M. M.: A two-tracer (²¹⁰Po-²³⁴Th) approach to distinguish
874 organic carbon and biogenic silica export flux in the Antarctic Circumpolar Current, *Deep. Res. Part I*
875 *Oceanogr. Res. Pap.*, 49, 101–120, [https://doi.org/10.1016/S0967-0637\(01\)00045-0](https://doi.org/10.1016/S0967-0637(01)00045-0), 2002.

876 Georg, R. B., Reynolds, B. C., Frank, M., and Halliday, A. N.: New sample preparation techniques for
877 the determination of Si isotopic compositions using MC-ICPMS, *Chem. Geol.*, 235, 95–104,
878 <https://doi.org/10.1016/j.chemgeo.2006.06.006>, 2006.

879 Giering, S. L. C., Cavan, E. L., Basedow, S. L., Briggs, N., Burd, A. B., Darroch, L. J., Guidi, L., Irisson, J.
880 O., Iversen, M. H., Kiko, R., Lindsay, D., Marcolin, C. R., McDonnell, A. M. P., Möller, K. O., Passow, U.,
881 Thomalla, S., Trull, T. W., and Waite, A. M.: Sinking Organic Particles in the Ocean—Flux Estimates
882 From in situ Optical Devices, *Front. Mar. Sci.*, 6, <https://doi.org/10.3389/fmars.2019.00834>, 2020.

883 Gleiber, M. R., Steinberg, D. K., and Ducklow, H. W.: Time series of vertical flux of zooplankton fecal
884 pellets on the continental shelf of the western Antarctic Peninsula, *Mar. Ecol. Prog. Ser.*, 471, 23–36,
885 <https://doi.org/10.3354/meps10021>, 2012.

886 Glibert, P. M., Wilkerson, F. P., Dugdale, R. C., Raven, J. A., Dupont, C. L., Leavitt, P. R., Parker, A. E.,
887 Burkholder, J. M., and Kana, T. M.: Pluses and minuses of ammonium and nitrate uptake and
888 assimilation by phytoplankton and implications for productivity and community composition, with
889 emphasis on nitrogen-enriched conditions, *Limnol. Oceanogr.*, 61, 165–197,
890 <https://doi.org/10.1002/lno.10203>, 2016.

891 González, H. E., Daneri, G., Iriarte, J. L., Yannicelli, B., Menschel, E., Barría, C., Pantoja, S., and
892 Lizárraga, L.: Carbon fluxes within the epipelagic zone of the Humboldt Current System off Chile: The
893 significance of euphausiids and diatoms as key functional groups for the biological pump, *Prog.*
894 *Oceanogr.*, 83, 217–227, <https://doi.org/10.1016/j.pocean.2009.07.036>, 2009.

895 Grasse, P., Brzezinski, M. A., Cardinal, D., De Souza, G. F., Andersson, P., Closset, I., Cao, Z., Dai, M.,
896 Ehlert, C., Estrade, N., François, R., Frank, M., Jiang, G., Jones, J. L., Kooijman, E., Liu, Q., Lu, D.,
897 Pahnke, K., Ponzevera, E., Schmitt, M., Sun, X., Sutton, J. N., Thil, F., Weis, D., Wetzels, F., Zhang, A.,

898 Zhang, J., and Zhang, Z.: GEOTRACES inter-calibration of the stable silicon isotope composition of
899 dissolved silicic acid in seawater, *J. Anal. At. Spectrom.*, 32, 562–578,
900 <https://doi.org/10.1039/c6ja00302h>, 2017.

901 Grasse, P., Haynert, K., Doering, K., Geilert, S., Jones, J. L., Brzezinski, M. A., and Frank, M.: Controls
902 on the Silicon Isotope Composition of Diatoms in the Peruvian Upwelling, *Front. Mar. Sci.*, 8, 1–15,
903 <https://doi.org/10.3389/fmars.2021.697400>, 2021.

904 Grossart, H. P., Kiørboe, T., Tang, K., and Ploug, H.: Bacterial colonization of particles: Growth and
905 interactions, *Appl. Environ. Microbiol.*, 69, 3500–3509, [https://doi.org/10.1128/AEM.69.6.3500-](https://doi.org/10.1128/AEM.69.6.3500-3509.2003)
906 3509.2003, 2003.

907 Hansman, R. L. and Sessions, A. L.: Measuring the in situ carbon isotopic composition of distinct
908 marine plankton populations sorted by flow cytometry, *Limnol. Oceanogr. Methods*, 14, 87–99,
909 <https://doi.org/10.1002/lom3.10073>, 2016.

910 Hasle, G. R. and Syvertsen, E. E.: Chapter 2 – Marine Diatoms, in: *Identifying Marine Phytoplankton*,
911 edited by: Tomas, C. R., Academic Press, San Diego, 5–385, 1997.

912 Hatton, J. E., Hendry, K. R., Hawkings, J. R., Wadham, J. L., Opfergelt, S., Kohler, T. J., Yde, J. C., Stibal,
913 M., and Žárský, J. D.: Silicon isotopes in Arctic and sub-Arctic glacial meltwaters: The role of
914 subglacial weathering in the silicon cycle, *Proc. R. Soc. A Math. Phys. Eng. Sci.*, 475,
915 <https://doi.org/10.1098/rspa.2019.0098>, 2019.

916 Hawco, N. J., Barone, B., Church, M. J., Babcock-Adams, L., Repeta, D. J., Wear, E. K., Foreman, R. K.,
917 Björkman, K. M., Bent, S., Van Mooy, B. A. S., Sheyn, U., DeLong, E. F., Acker, M., Kelly, R. L., Nelson,
918 A., Ranieri, J., Clemente, T. M., Karl, D. M., and John, S. G.: Iron Depletion in the Deep Chlorophyll
919 Maximum: Mesoscale Eddies as Natural Iron Fertilization Experiments, *Global Biogeochem. Cycles*,
920 35, 1–18, <https://doi.org/10.1029/2021GB007112>, 2021.

921 Hendry, K. R. and Brzezinski, M. A.: Using silicon isotopes to understand the role of the Southern
922 Ocean in modern and ancient biogeochemistry and climate, *Quat. Sci. Rev.*, 89, 13–26,
923 <https://doi.org/10.1016/j.quascirev.2014.01.019>, 2014.

924 Hendry, K. R. and Robinson, L. F.: The relationship between silicon isotope fractionation in sponges
925 and silicic acid concentration: Modern and core-top studies of biogenic opal, *Geochim. Cosmochim.*
926 *Acta*, 81, 1–12, <https://doi.org/10.1016/j.gca.2011.12.010>, 2012.

927 Henley, S. F., Annett, A. L., Ganeshram, R. S., Carson, D. S., Weston, K., Crosta, X., Tait, A., Dougans,
928 J., Fallick, A. E., and Clarke, A.: Factors influencing the stable carbon isotopic composition of
929 suspended and sinking organic matter in the coastal Antarctic sea ice environment, *Biogeosciences*,
930 9, 1137–1157, <https://doi.org/10.5194/bg-9-1137-2012>, 2012.

931 Hillebrand, H., Dürselen, C. D., Kirschtel, D., Pollinger, U., and Zohary, T.: Biovolume calculation for
932 pelagic and benthic microalgae, *J. Phycol.*, 35, 403–424, [https://doi.org/10.1046/j.1529-](https://doi.org/10.1046/j.1529-8817.1999.3520403.x)
933 8817.1999.3520403.x, 1999.

934 Honjo, S., Francois, R., Manganini, S., Dymond, J., and Collier, R.: Particle fluxes to the interior of the
935 Southern Ocean in the Western Pacific sector along 170°W, *Deep. Res. Part II*, 47, 3521–3548,
936 [https://doi.org/10.1016/S0967-0645\(00\)00077-1](https://doi.org/10.1016/S0967-0645(00)00077-1), 2000.

937 Iversen, M. H., Pakhomov, E. A., Hunt, B. P. V., Jagt, H. Van Der, Wolf-gladrow, D., and Klaas, C.:
938 Sinkers or floaters? Contribution from salp pellets to the export flux during a large bloom event in
939 the Southern Ocean, *Deep Sea Res. Part II Top. Stud. Oceanogr.*, 138, 116–125,
940 <https://doi.org/10.1016/j.dsr2.2016.12.004>, 2017.

941 Kiørboe, T., Tang, K., Grossart, H. P., and Ploug, H.: Dynamics of microbial communities on marine

942 snow aggregates: Colonization, growth, detachment, and grazing mortality of attached bacteria,
943 *Appl. Environ. Microbiol.*, 69, 3036–3047, <https://doi.org/10.1128/AEM.69.6.3036-3047.2003>, 2003.

944 Korb, R. E., Whitehouse, M. J., Atkinson, A., and Thorpe, S.: Magnitude and maintenance of the
945 phytoplankton bloom at South Georgia: a naturally iron-replete environment, *Mar. Ecol. Prog. Ser.*,
946 368, 75–91, <https://doi.org/10.3354/meps07525>, 2008.

947 Korb, R. E., Whitehouse, M. J., Ward, P., Gordon, M., Venables, H. J., and Poulton, A. J.: Regional and
948 seasonal differences in microplankton biomass, productivity, and structure across the Scotia Sea:
949 Implications for the export of biogenic carbon, *Deep Sea Res. Part II Top. Stud. Oceanogr.*, 59–60,
950 67–77, <https://doi.org/10.1016/j.dsr2.2011.06.006>, 2012.

951 Kwon, E., Primeau, F., and Sarmiento, J.: The impact of remineralization depth on the air-sea carbon
952 balance, *Nat. Geosci.*, 2, 630–635, 2009.

953 De La Rocha, C. L., Brzezinski, M. A., and DeNiro, M. J.: Fractionation of silicon isotopes by marine
954 diatoms during biogenic silica formation, *Geochim. Cosmochim. Acta*, 61, 5051–5056,
955 [https://doi.org/10.1016/S0016-7037\(97\)00300-1](https://doi.org/10.1016/S0016-7037(97)00300-1), 1997.

956 Manno, C., Stowasser, G., Enderlein, P., Fielding, S., and Tarling, G. A.: The contribution of
957 zooplankton faecal pellets to deep-carbon transport in the Scotia Sea (Southern Ocean),
958 *Biogeosciences*, 12, 1955–1965, <https://doi.org/10.5194/bg-12-1955-2015>, 2015.

959 Manno, C., Fielding, S., Stowasser, G., Murphy, E. J., and Thorpe, S. E.: Continuous moulting by
960 Antarctic krill drives major, *Nat. Commun.*, 16, 6051, <https://doi.org/10.1038/s41467-020-19956-7>,
961 2020.

962 Matano, R. P., Combes, V., Young, E. F., and Meredith, M. P.: Modeling the Impact of Ocean
963 Circulation on Chlorophyll Blooms Around South Georgia, *Southern Ocean*, *J. Geophys. Res. Ocean.*,
964 125, 1–18, <https://doi.org/10.1029/2020JC016391>, 2020.

965 Medlin, L. K. and Priddle, J.: *Polar marine diatoms*, British Antarctic Survey, Cambridge, UK, 214 pp.,
966 1990.

967 Meyerink, S. W., Boyd, P. W., Maher, W. A., Milne, A., Strzepek, R., and Ellwood, M. J.: Putting the
968 silicon cycle in a bag: Field and mesocosm observations of silicon isotope fractionation in subtropical
969 waters east of New Zealand, *Mar. Chem.*, 213, 1–12,
970 <https://doi.org/10.1016/j.marchem.2019.04.008>, 2019.

971 Michener, R. and Lajtha, K.: *Stable Isotopes in Ecology and Environmental Science: Second Edition*,
972 1–566 pp., <https://doi.org/10.1002/9780470691854>, 2008.

973 Minagawa, M. and Wada, E.: Stepwise enrichment of ^{15}N along food chains: Further evidence and
974 the relation between $\delta^{15}\text{N}$ and animal age, *Geochim. Cosmochim. Acta*, 48, 1135–1140,
975 [https://doi.org/10.1016/0016-7037\(84\)90204-7](https://doi.org/10.1016/0016-7037(84)90204-7), 1984.

976 Mincks, S. L., Smith, C. R., Jeffreys, R. M., and Sumida, P. Y. G.: Trophic structure on the West
977 Antarctic Peninsula shelf: Detritivory and benthic inertia revealed by $\delta^{13}\text{C}$ and $\delta^{15}\text{N}$ analysis, *Deep*,
978 *Res. Part II Top. Stud. Oceanogr.*, 55, 2502–2514, <https://doi.org/10.1016/j.dsr2.2008.06.009>, 2008.

979 Montoya, J. P.: Natural abundance of ^{15}N in marine planktonic ecosystems, in: *Stable Isotopes in*
980 *Ecology and Environmental Science: Second Edition*, edited by: Michener, R. and Lajtha, K., Blackwell
981 Publishing, 1–566, <https://doi.org/10.1002/9780470691854>, 2007.

982 Moore, J. K., Abbott, M. R., and Richman, J. G.: Location and dynamics of the Antarctic Polar Front
983 from satellite sea surface temperature data, *J. Geophys. Res. Ocean.*, 104, 3059–3073,
984 <https://doi.org/10.1029/1998JC900032>, 1999.

985 Ng, H. C., Cassarino, L., Pickering, R. A., Woodward, E. M. S., Hammond, S. J., and Hendry, K. R.:
986 Sediment efflux of silicon on the Greenland margin and implications for the marine silicon cycle,
987 *Earth Planet. Sci. Lett.*, 529, 115877, <https://doi.org/10.1016/j.epsl.2019.115877>, 2020.

988 Nielsdóttir, M. C., Bibby, T. S., Moore, C. M., Hinz, D. J., Sanders, R., Whitehouse, M., Korb, R., and
989 Achterberg, E. P.: Seasonal and spatial dynamics of iron availability in the Scotia Sea, *Mar. Chem.*,
990 130–131, 62–72, <https://doi.org/10.1016/j.marchem.2011.12.004>, 2012.

991 Opfergelt, S. and Delmelle, P.: Silicon isotopes and continental weathering processes: Assessing
992 controls on Si transfer to the ocean, *Comptes Rendus - Geosci.*, 344, 723–738,
993 <https://doi.org/10.1016/j.crte.2012.09.006>, 2012.

994 Orsi, H., Whitworth III, T., and Nowlin Jr, W. D.: On the meridional extent and fronts of the Antarctic
995 Circumpolar Current, *Deep Sea Res. Part I Oceanogr. Res. Pap.*, 42, 641–673,
996 [https://doi.org/10.1016/0967-0637\(95\)00021-W](https://doi.org/10.1016/0967-0637(95)00021-W), 1995.

997 Passow, U. and De La Rocha, C. L.: Accumulation of mineral ballast on organic aggregates, *Global*
998 *Biogeochem. Cycles*, 20, 1–7, <https://doi.org/10.1029/2005GB002579>, 2006.

999 Pauli, N.-C., Flintrop, C. M., Konrad, C., Pakhomov, E. A., Swoboda, S., Koch, F., Wang, X.-L., Zhang, J.-
1000 C., Brierley, A. S., Bernasconi, M., Meyer, B., and Iversen, M. H.: Krill and salp faecal pellets
1001 contribute equally to the carbon flux at the Antarctic Peninsula, *Nat. Commun.*, 12, 7168,
1002 <https://doi.org/10.1038/s41467-021-27436-9>, 2021.

1003 Ploug, H., Iversen, M. H., and Fischer, G.: Ballast, sinking velocity, and apparent diffusivity within
1004 marine snow and zooplankton fecal pellets: Implications for substrate turnover by attached bacteria,
1005 *Limnol. Oceanogr.*, 53, 1878–1886, 2008.

1006 Popp, B. N., Laws, E. A., Bidigare, R. R., Dore, J. E., Hanson, K. L., and Wakeham, S. G.: Effect of
1007 phytoplankton cell geometry on carbon isotopic fractionation, *Geochim. Cosmochim. Acta*, 62, 69–
1008 77, [https://doi.org/10.1016/S0016-7037\(97\)00333-5](https://doi.org/10.1016/S0016-7037(97)00333-5), 1998.

1009 Popp, B. N., Trull, T., Kenig, F., Wakeham, S. G., Rust, T. M., Tilbrook, B., Griffiths, F. B., Wright, S. W.,
1010 Marchant, H. J., Bidigare, R. R., and Laws, E. A.: Controls on the carbon isotopic composition of
1011 Southern Ocean phytoplankton, *Global Biogeochem. Cycles*, 13, 827–843,
1012 <https://doi.org/10.1029/1999GB900041>, 1999.

1013 Priddle, J. and Fryxell, G.: Handbook of the common plankton diatoms of the Southern Ocean:
1014 Centrales except the genus *Thalassiosira*, British Antarctic Survey, Cambridge, UK, 159 pp., 1985.

1015 Rau, G. H., Froelich, P. N., Takahashi, T., and J., D. M. D.: Does sedimentary organic $\delta^{13}\text{C}$ record
1016 variations in quaternary ocean $[\text{CO}_2(\text{aq})]$, *Paleoceanography*, 6, 335–347, 1991.

1017 Raven, J. A.: Inorganic Carbon Acquisition by Marine Autotrophs, *Adv. Bot. Res.*, 27, 85–209,
1018 [https://doi.org/10.1016/S0065-2296\(08\)60281-5](https://doi.org/10.1016/S0065-2296(08)60281-5), 1997.

1019 Rembauville, M., Blain, S., Armand, L., Quéguiner, B., and Salter, I.: Export fluxes in a naturally iron-
1020 fertilized area of the Southern Ocean – Part 2: Importance of diatom resting spores and faecal
1021 pellets for export, *Biogeosciences*, 12, 3171–3195, <https://doi.org/10.5194/bg-12-3171-2015>, 2015.

1022 Rembauville, M., Manno, C., Tarling, G. A., Blain, S., and Salter, I.: Strong contribution of diatom
1023 resting spores to deep-sea carbon transfer in naturally iron-fertilized waters downstream of South
1024 Georgia, *Deep. Res. Part I*, 115, 22–35, <https://doi.org/10.1016/j.dsr.2016.05.002>, 2016.

1025 Reynolds, B. C., Aggarwal, J., André, L., Baxter, D., Beucher, C., Brzezinski, M. A., Engström, E., Georg,
1026 R. B., Land, M., Leng, M. J., Opfergelt, S., Rodushkin, I., Sloane, H. J., Van Den Boorn, S. H. J. M.,
1027 Vroon, P. Z., and Cardinal, D.: An inter-laboratory comparison of Si isotope reference materials, J.

- 1028 Anal. At. Spectrom., 22, 561–568, <https://doi.org/10.1039/b616755a>, 2007.
- 1029 Roberts, K., Granum, E., Leegood, R. C., and Raven, J. A.: Carbon acquisition by diatoms, *Photosynth.*
1030 *Res.*, 93, 79–88, <https://doi.org/10.1007/s11120-007-9172-2>, 2007.
- 1031 Roca-Marti, M., Puigcorbé, V., Iversen, M. H., Rutgers van der Loeff, M., Klaas, C., Cheah, W.,
1032 Bracher, A., and Masqué, P.: High particulate organic carbon export during the decline of a vast
1033 diatom bloom in the Atlantic sector of the Southern Ocean, *Deep Sea Res. Part II Top. Stud.*
1034 *Oceanogr.*, 138, 102–115, <https://doi.org/10.1016/j.dsr2.2015.12.007>, 2017.
- 1035 Salter, I., Kemp, A. E. S. S., Moore, C. M., Lampitt, R. S., Wolff, G. A., and Holtvoeth, J.: Diatom resting
1036 spore ecology drives enhanced carbon export from a naturally iron-fertilized bloom in the Southern
1037 Ocean, *Global Biogeochem. Cycles*, 26, 1–17, <https://doi.org/10.1029/2010GB003977>, 2012.
- 1038 Sathyendranath, S., Brewin, R., Brockmann, C., Brotas, V., Calton, B., Chuprin, A., Cipollini, P., Couto,
1039 A., Dingle, J., Doerffer, R., Donlon, C., Dowell, M., Farman, A., Grant, M., Groom, S., Horseman, A.,
1040 Jackson, T., Krasemann, H., Lavender, S., Martinez-Vicente, V., Mazeran, C., Mélin, F., Moore, T.,
1041 Müller, D., Regner, P., Roy, S., Steele, C., Steinmetz, F., Swinton, J., Taberner, M., Thompson, A.,
1042 Valente, A., Zühlke, M., Brando, V., Feng, H., Feldman, G., Franz, B., Frouin, R., Gould, R., Hooker, S.,
1043 Kahru, M., Kratzer, S., Mitchell, B., Muller-Karger, F., Sosik, H., Voss, K., Werdell, J., and Platt, T.: An
1044 Ocean-Colour Time Series for Use in Climate Studies: The Experience of the Ocean-Colour Climate
1045 Change Initiative (OC-CCI), *Sensors*, 19, 4285, <https://doi.org/10.3390/s19194285>, 2019.
- 1046 Sathyendranath, S., Jackson, T., Brockmann, C., Brotas, V., Calton, B., Chuprin, A., Clements, O.,
1047 Cipollini, P., Danne, O., Dingle, J., Donlon, C., Grant, M., Groom, S., Krasemann, H., Lavender, S.,
1048 Mazeran, C., Mélin, F., Müller, D., Steinmetz, F., Valente, A., Zühlke, M., Feldman, G., Franz, B.,
1049 Frouin, R., Werdell, J., and Platt, T.: ESA Ocean Colour Climate Change Initiative (Ocean_Colour_cci):
1050 Version 5.0 Data, NERC EDS Cent. *Environ. Data Anal.*,
1051 <https://doi.org/10.5285/1dbe7a109c0244aaad713e078fd3059a>, 2021.
- 1052 Schmidt, K., Atkinson, A., Stübing, D., McClelland, J. W., Montoya, J. P., and Voss, M.: Trophic
1053 relationships among Southern Ocean copepods and krill: Some uses and limitations of a stable
1054 isotope approach, *Limnol. Oceanogr.*, 48, 277–289, <https://doi.org/10.4319/lo.2003.48.1.0277>,
1055 2003.
- 1056 Scott, F. J. and Marchant, H. J. (Eds.): *Antarctic Marine Protists*, Australian Biological Resources
1057 Study, Canberra, 2005.
- 1058 Shen, C., Dupont, C. L., and Hopkinson, B. M.: The diversity of CO₂-concentrating mechanisms in
1059 marine diatoms as inferred from their genetic content, *J. Exp. Bot.*, 68, 3937–3948,
1060 <https://doi.org/10.1093/jxb/erx163>, 2017.
- 1061 Sigman, D. M. and Fripiat, F.: Nitrogen isotopes in the ocean, *Encycl. Ocean Sci.*, 263–278,
1062 <https://doi.org/10.1016/B978-0-12-409548-9.11605-7>, 2019.
- 1063 Smetacek, V., Assmy, P., and Henjes, J.: The role of grazing in structuring Southern Ocean pelagic
1064 ecosystems and biogeochemical cycles, *Antarct. Sci.*, 16, 541–558,
1065 <https://doi.org/10.1017/S0954102004002317>, 2004.
- 1066 Strickland, J. and Parsons, T.: *A Practical Handbook of Seawater Analysis*, Fisheries Research Board of
1067 Canada, 405 pp., <https://doi.org/10.2307/1979241>, 1972.
- 1068 Sutton, J. N., Varela, D. E., Brzezinski, M. A., and Beucher, C. P.: Species-dependent silicon isotope
1069 fractionation by marine diatoms, *Geochim. Cosmochim. Acta*, 104, 300–309,
1070 <https://doi.org/10.1016/j.gca.2012.10.057>, 2013.
- 1071 Tamelander, T., Søreide, J. E., Hop, H., and Carroll, M. L.: Fractionation of stable isotopes in the Arctic

- 1072 marine copepod *Calanus glacialis*: Effects on the isotopic composition of marine particulate organic
1073 matter, *J. Exp. Mar. Bio. Ecol.*, 333, 231–240, <https://doi.org/10.1016/j.jembe.2006.01.001>, 2006.
- 1074 Thorpe, S. E., Heywood, K. J., Brandon, M. A., and Stevens, D. P.: Variability of the southern Antarctic
1075 Circumpolar Current front north of South Georgia, *J. Mar. Syst.*, 37, 87–105,
1076 [https://doi.org/10.1016/S0924-7963\(02\)00197-5](https://doi.org/10.1016/S0924-7963(02)00197-5), 2002.
- 1077 Torres Valdés, S., Painter, S. C., Martin, A. P., Sanders, R., and Felden, J.: Data compilation of fluxes
1078 of sedimenting material from sediment traps in the Atlantic ocean, *Earth Syst. Sci. Data*, 6, 123–145,
1079 <https://doi.org/10.5194/essd-6-123-2014>, 2014.
- 1080 Trimborn, S., Wolf-Gladrow, D., Richter, K. U., and Rost, B.: The effect of pCO₂ on carbon acquisition
1081 and intracellular assimilation in four marine diatoms, *J. Exp. Mar. Bio. Ecol.*, 376, 26–36,
1082 <https://doi.org/10.1016/j.jembe.2009.05.017>, 2009.
- 1083 Trull, T. W. and Armand, L.: Insights into Southern Ocean carbon export from the $\delta^{13}C$ of particles
1084 and dissolved inorganic carbon during the SOIREE iron release experiment, *Deep. Res. Part II Top.*
1085 *Stud. Oceanogr.*, 48, 2655–2680, [https://doi.org/10.1016/S0967-0645\(01\)00013-3](https://doi.org/10.1016/S0967-0645(01)00013-3), 2001.
- 1086 Trull, T. W., Bray, S. G., Manganimi, S. J., Honjo, S., and François, R.: of the Southern Ocean , south of
1087 Australia with traps fluxes were high at all the sites mass g organic carbon m⁻¹ at-1000 m , assuming
1088 minimal flux outside the Subantarctic Front with one trap at 3080 m , and at -54øS in the Polar
1089 Frontal Zone (PF • Z), *J. Geophys. Res.*, 106, 31,489-31,509, 2001.
- 1090 Tuerena, R. E., Ganeshram, R. S., Humphreys, M. P., Browning, T. J., Bouman, H., and Piotrowski, A.
1091 P.: Isotopic fractionation of carbon during uptake by phytoplankton across the South Atlantic
1092 subtropical convergence, *Biogeosciences*, 16, 3621–3635, <https://doi.org/10.5194/bg-16-3621-2019>,
1093 2019.
- 1094 Volk, T. and Hoffert, M. I.: Ocean Carbon Pumps: Analysis of relative strengths and efficiencies in
1095 ocean driven atmospheric CO₂ changes, in: *The carbon cycle and atmospheric CO₂: Natural variations*
1096 *Archean to Present*, edited by: Sundquist, E. T. and Broecker, W. S., American Geophysical Union,
1097 Washington, DC, 99–110, 1985.
- 1098 Wada, E. and Hattori, A.: Nitrogen isotope effects in the assimilation of inorganic nitrogenous
1099 compounds by marine diatoms, *Geomicrobiol. J.*, 1, 85–101,
1100 <https://doi.org/10.1080/01490457809377725>, 1978.
- 1101 Wada, E., Terazaki, M., Kabaya, Y., and Nemoto, T.: ¹⁵N and ¹³C abundances in the Antarctic Ocean
1102 with emphasis on the biogeochemical structure of the food web, *Deep Sea Res. Part A, Oceanogr.*
1103 *Res. Pap.*, 34, 829–841, [https://doi.org/10.1016/0198-0149\(87\)90039-2](https://doi.org/10.1016/0198-0149(87)90039-2), 1987.
- 1104 Ward, J. P. J., Hendry, K. R., Arndt, S., Faust, J. C., Freitas, F. S., Henley, S. F., Krause, J. W., März, C.,
1105 Ng, H. C., Pickering, R. A., and Tessin, A. C.: Stable silicon isotopes uncover a mineralogical control on
1106 the benthic silicon cycle in the Arctic Barents Sea, *Geochim. Cosmochim. Acta*, 329, 206–230,
1107 <https://doi.org/10.1016/j.gca.2022.05.005>, 2022.
- 1108 Weir, I., Fawcett, S., Smith, S., Walker, D., Bornman, T., and Fietz, S.: Winter biogenic silica and
1109 diatom distributions in the Indian sector of the Southern Ocean, *Deep. Res. Part I Oceanogr. Res.*
1110 *Pap.*, 166, 103421, <https://doi.org/10.1016/j.dsr.2020.103421>, 2020.
- 1111 Wetzel, F., de Souza, G. F., and Reynolds, B. C.: What controls silicon isotope fractionation during
1112 dissolution of diatom opal?, *Geochim. Cosmochim. Acta*, 131, 128–137,
1113 <https://doi.org/10.1016/j.gca.2014.01.028>, 2014.
- 1114 White, W. M., Albarède, F., and Télouk, P.: High-precision analysis of Pb isotope ratios by multi-
1115 collector ICP-MS, *Chem. Geol.*, 167, 257–270, [https://doi.org/10.1016/S0009-2541\(99\)00182-5](https://doi.org/10.1016/S0009-2541(99)00182-5),

1116 2000.

1117 Whitehouse, M. J., Priddle, J., Trathan, P. N., and Brandon, M. A.: Substantial open-ocean
1118 phytoplankton blooms to the north of South Georgia, South Atlantic, during summer 1994, Mar.
1119 Ecol. Prog. Ser., 140, 187–197, <https://doi.org/10.3354/meps140187>, 1996.

1120 Young, J. N., Heureux, A. M. C., Sharwood, R. E., Rickaby, R. E. M., Morel, F. M. M., and Whitney, S.
1121 M.: Large variation in the Rubisco kinetics of diatoms reveals diversity among their carbon-
1122 concentrating mechanisms, J. Exp. Bot., 67, 3445–3456, <https://doi.org/10.1093/jxb/erw163>, 2016.

1123